



**UNIVERSIDAD DE INVESTIGACIÓN DE TECNOLOGÍA
EXPERIMENTAL YACHAY**

Escuela de Ciencias Físicas y Nanotecnología

**TÍTULO: Usage of High Energy Photons to understand the
interaction between CoFe_2O_4 , chitosan, graphene, and glyphosate to
describe its removal efficiency from water.**

Trabajo de integración curricular presentado como requisito para la
obtención
del título de Físico

Autor:

Salguero Pesantez Orlando Daniel

Tutor:

Ph.D. – Reinoso Carlos

Co-tutor:

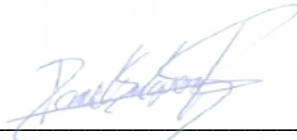
Ph.D. – Briceño Sarah

Urcuquí, julio 2023

AUTORÍA

Yo, **Salguero Pesantez Orlando Daniel**, con cédula de identidad 1724830896. declaro que las ideas, juicios, valoraciones, interpretaciones, consultas bibliográficas, definiciones y conceptualizaciones expuestas en el presente trabajo; así cómo, los procedimientos y herramientas utilizadas en la investigación, son de absoluta responsabilidad de el/la autora (a) del trabajo de integración curricular. Así mismo, me acojo a los reglamentos internos de la Universidad de Investigación de Tecnología Experimental Yachay.

Urcuquí, julio 2023.



Orlando Daniel Salguero Pesantez
CI: 1724830896

AUTORIZACIÓN DE PUBLICACIÓN

Yo, **Salguero Pesantez Orlando Daniel**, con cédula de identidad 1724830896, cedo a la Universidad de Investigación de Tecnología Experimental Yachay, los derechos de publicación de la presente obra, sin que deba haber un reconocimiento económico por este concepto. Declaro además que el texto del presente trabajo de titulación no podrá ser cedido a ninguna empresa editorial para su publicación u otros fines, sin contar previamente con la autorización escrita de la Universidad.

Asimismo, autorizo a la Universidad que realice la digitalización y publicación de este trabajo de integración curricular en el repositorio virtual, de conformidad a lo dispuesto en el Art. 144 de la Ley Orgánica de Educación Superior

Urcuquí, julio 2023.



Orlando Daniel Salguero Pesantez
CI: 1724830896

Acknowledgements

I want to express my deepest gratitude to all my professors at Yachay Tech University who have accompanied me during this 5-year journey with their support and knowledge. This goes especially to my advisor Dr. Carlos Reinoso who taught me about X-ray photoelectron spectroscopy and provided me with the necessary tools to understand and develop this project. In the same way, I want to thank my co-advisor Dr. Sarah Briceño who motivated me to continue with this work and guided me in improving this work. Also, I want to thank all the members of the School of Physical Sciences and Nanotechnology that helped me during this process. I am sure they are excellent people who made me feel confident that I was in the right place.

And of course, I am grateful to my parents Orlando and Martha, who raised me to be an excellent person guiding me through every moment of my life. To my siblings Gabriel and Linda, who taught me what true and unconditional love is. To my grandparents, and my family who never wavered in their support cheering me up through thick and thin. For you who taught me that I should never give up no matter what, and made me understand that pursuing my dreams is the most important thing I should do. I am sure that without them I would have not been able to be the person I am now.

Finally, to the people I met in Yachay Tech Eder, Sebastian, Angie, Daniela, and everyone who I can truly call friends who accompanied me during all these five years. I consider this university is a special place where you can be genuine and sincere with others. A place you can develop yourself both in a professional and personal way. Thanks to you all, I love the path I have chosen in my life, and I am pretty sure I will be an excellent scientist thanks to the things I have learned here. May this work will reflect a small part of what I was able to learn during this perilous path full of joy, and may it inspire the future me to continue in this scientific world. The pursuit of knowledge is a journey worth taking, and the rewards are as great as the challenges we face.

Orlando Daniel Salguero Pesantez

Dedication

This goes as well to Karolina, a special person who during all these five years has been part of my inspiration. Thank you for encouraging me, and reminding me that anything is possible if you invest in hard work, patience, and determination. For every achievement I obtained, for every mistake I made during these five years, and for every moment you were there to support me and put me back in the right place helping me grow as a person. To you who the universe in the infinite ocean of possibilities was kind enough to put in my path. I dedicate this work to you with all my love and appreciation.

Orlando Daniel Salguero Pesantez

Resumen

El glifosato (N-fosfonometilglicina) es el principal ingrediente activo de un conjunto de pesticidas comerciales más ampliamente utilizados a nivel mundial debido a su alta eficacia en la eliminación no selectiva de malezas. Existen varias preocupaciones ya que los aditivos del glifosato pueden contener diferentes sales y tensioactivos peligrosos para las personas y el medio ambiente. En este trabajo, se realiza un análisis de un nuevo nanocompuesto hecho de grafeno, quitosano y CoFe_2O_4 a través de varias técnicas espectroscópicas para determinar su actividad cuando se expone al glifosato como alternativa para eliminar este compuesto contaminante. En este trabajo se utilizan técnicas de espectroscopía de fotoelectrones de rayos X (XPS), así como espectroscopía infrarroja por transformada de Fourier (FTIR) y espectroscopía RAMAN para analizar las interacciones de unión entre cada uno de los componentes del nanocompuesto y el glifosato. A través del estudio del grafeno, quitosano, ferrita de cobalto y el nanocompuesto con glifosato utilizando estas técnicas, fue posible encontrar que existe una interacción que ocurre principalmente a través de los grupos carboxílicos y fosfato, mostrados principalmente en el análisis FTIR y XPS. Los resultados muestran que el nanocompuesto tiene una mayor interacción química con el glifosato en comparación con cada uno de los componentes, lo que hace que este nanocompuesto sea una buena alternativa como bioadsorbente para la eliminación del glifosato.

Palabras Clave: nanocompuesto, glifosato, grafeno, RAMAN, FTIR, XPS.

Abstract

Glyphosate (N-phosphonomethyl glycine) is the main active ingredient of a set of commercial pesticides most widely used globally due to its high effectiveness in removing weeds through non-discriminatory elimination. There exist several concerns since the additives of glyphosate may contain different salts and surfactants dangerous to people and the environment. In this work, an analysis of a novel nanocomposite made of graphene, chitosan, and CoFe_2O_4 is performed through various spectroscopy techniques to determine its activity when exposed to glyphosate as an alternative to remove this pollutant compound. X-ray photoelectron spectroscopy (XPS), as well as Fourier, transform infrared spectroscopy (FTIR), and RAMAN spectroscopy techniques are used in this work to analyze the binding interactions between each one of the components of the nanocomposite with the glyphosate. Through the study of Graphene, Chitosan, Cobalt ferrite, and the nanocomposite with Glyphosate using these techniques it was possible to find that there is an interaction occurring mainly through the carboxylic, and phosphate groups showed mainly in the FTIR and XPS analysis. The results show that the nanocomposite has a bigger chemical interaction with glyphosate compared to each one of the components which makes this nanocomposite a good alternative as a bio-adsorbent for glyphosate removal.

Keywords: nanocomposite, glyphosate, graphene, RAMAN, FTIR, XPS.

Contents

List of Figures	xii
List of Tables	xiv
1 Introduction	1
1.1 Problem Statement	3
1.2 General Objectives	3
1.3 Specific Objectives	3
2 Theoretical Background	5
2.1 Pesticides	5
2.2 Glyphosate	5
2.2.1 Environmental Impact	7
2.2.2 Health Issues	8
2.3 Carbon Nanomaterials	8
2.3.1 Graphene	8
2.3.2 Characterization of Graphene	10
2.4 Chitosan	10
2.5 Magnetic Nanoparticles	10
2.5.1 Cobalt Ferrite Nanoparticles	12
2.6 Nanocomposite	13
2.6.1 CoFe ₂ O ₄ , Graphene, and Chitosan nanocomposite	13
2.7 Raman Spectroscopy	14
2.7.1 Raman working principle	14
2.8 Fourier Transform Infrared Spectroscopy (FTIR)	16

2.8.1	FTIR working principle	16
2.9	X-Ray Photoelectron Spectroscopy	17
2.9.1	XPS Data Analysis	20
2.9.2	Process of XPS spectra fitting	21
3	Methodology	23
3.1	Sample Preparation	23
3.2	Molecular and Structural Characterization	24
3.2.1	Raman Spectroscopy	24
3.2.2	Fourier Transform Infrared Spectroscopy	25
3.2.3	X-ray photoelectron spectroscopy	26
4	Results & Discussion	29
4.1	Raman Spectroscopy	29
4.2	Fourier Transform Infrared Spectroscopy (FTIR)	32
4.3	X-ray Photoelectron Spectroscopy (XPS)	35
4.3.1	Interaction Glyphosate-Graphene (Gly-Gr)	36
4.3.2	Interaction Glyphosate-Chitosan (Gly-Cs)	38
4.3.3	Interaction Glyphosate-Cobalt Ferrite (Gly-Co)	41
4.3.4	Interaction Glyphosate-Nanocomposite (Gly-Nc)	44
5	Conclusions & Outlook	49
	Bibliography	51

List of Figures

2.1	Glyphosate Chemical Structure	6
2.2	Geographic distribution of Glyphosate contamination.	7
2.3	Carbon materials 2D, and 3D structure	9
2.4	Chemical structure of Chitin/Chitosan	11
2.5	Molecular structure of CoFe–2O–4	12
2.6	RAMAN Jablonski diagram	15
2.7	Diagram of Michelson interferometer	17
2.8	Photoemission Three-step model	18
2.9	XPS schematic representation.	19
2.10	C1s, and O1s High-resolution XPS samples.	20
3.1	Nanocomposite diagram of fabrication	24
3.2	RAMAN Physics Lab, Yachay Tech University	25
3.3	FTIR Biology Yachay Tech University	26
3.4	XPS Physics Lab, Yachay Tech University	27
4.1	RAMAN spectrum for Gly-Nc, Gly, Nc, CoFe ₂ O ₄ , Gr, and Cs.	30
4.2	Raman spectrum for the interaction of the Gr, Cs, Co, and Nc with Gly.	33
4.3	850cm ⁻¹ Fingerprint region for Gly-Nc, Gly, Nc, CoFe ₂ O ₄ , Gr, and Cs.	34
4.4	850 cm ⁻¹ Fingerprint region for Gly-Nc, Gly, Nc, CoFe ₂ O ₄ , Gr, and Cs.	35
4.5	XPS Survey spectra for the Gly-Gr interaction.	36
4.6	XPS high resolution spectrum for the Gly-Gr interaction.	37
4.7	XPS survey for the Gly-Cs interaction.	39
4.8	XPS high-resolution spectrum for the Gly-Cs interaction	40
4.9	XPS survey spectrum for the Gly-Co interaction.	42

4.10 XPS high resolution spectrum for the Gly-Co interaction.	43
4.11 XPS survey spectrum for the Gly-Nc interaction.	45
4.12 XPS high resolution spectrum for the Gly-Nc interaction.	47

List of Tables

4.1	RAMAN shifts for Gly-Nc, Gly, Nc, CoFe ₂ O ₄ , Gr, and Cs.	31
4.2	C1s atomic concentration for the Gly-Gr interaction	38
4.3	C1s atomic concentrations for the Gly-Cs interaction.	41
4.4	C1s atomic concentrations for the Gly-Co interaction.	43
4.5	O1s atomic concentrations for the Gly-Co interaction.	44
4.7	O1s atomic concentrations for the Gly-Nc interaction.	46
4.6	C1s atomic concentrations for the Gly-Nc interaction.	46

Chapter 1

Introduction

The global need for food supply and the increment of crop yield around the world, has widespread, in farmers, to have turned to pesticides to protect their crops from pests and diseases. However, the use of these chemicals comes with consequences. One pesticide, in particular, is known for its effectiveness in controlling illegal crops, but we must consider the long-term impact on our environment and health. Glyphosate (N-phosphonomethyl glycine) is the main active ingredient of a set of commercial pesticides used due to its high effectiveness in removing weeds through non-discriminatory elimination.¹ This also helps in the wide-spreading of planting which is genetically modified to resist glyphosate-based pesticides. The concern about the usage of glyphosate compounds has been growing in recent years due to its possible environmental impacts, especially on human health due to its toxicity.² The mechanisms of toxicity of glyphosate-based formulations remain a topic of various research, and it is known that commercial formulations may contain different salts and surfactants that vary in nature and concentration.³ Surfactant ingestion and exposition can be dangerous to people since amine surfactants are strongly alkaline, and corrosive causing multiple organ failures.³

In Ecuador, pesticides containing glyphosate formulations have been used in aircraft fumigation as a counter-measurement to fight illegal crops in the borders with Colombia, especially those caused by drug trafficking operations.⁴ It is reported in an article from 1988 that glyphosate compounds are reduced to smaller molecules but not fully degraded by microorganisms and plants into carbon dioxide, phosphates, and water that can pollute nearby water sources.⁵ Due to the complications to human health, harmful effects, and illness caused by glyphosate pesticides in near-populated areas, a great concern about solutions to prevent these cases has appeared. Thus, an effective and trustful method is needed to remove this pollutant

from water in order to prevent diseases in humans. The adsorption and degradation processes are one of the most used methods to remove glyphosate from water being a simple, low-cost, easy operation process with high efficiency and high removal rates⁶. Nevertheless, the nature of the proposed adsorbent material may affect the adsorption process along with its performance which can also depend on the concentration of glyphosate, pH, temperature, and the presence of additives like surfactants. Several researchers have used nanomaterials as an adsorbent material for glyphosate pesticides like ZnO, goethite, and magnetic graphene hybrid composites.⁷ In order to develop an efficient process for removing glyphosate it is necessary to understand the individual components of commercial formulations and design efficient materials for its removal from water.⁸

In this work, the spectroscopy study of a simple magnetic nanocomposite including graphene, chitosan, and $CoFe_2O_4$ nanoparticles as a bio-adsorbent for commercial glyphosate remediation from water sources is proposed to understand the molecular interaction happening behind the adsorption process. The design of the nanocomposite was based on the properties that graphene shows like its wide surface area which enhances its adsorption efficiency.⁹ Since it is not easy to recover from the water after the process, while combined with chitosan, graphene gains hydrophilicity and bio-compatibility improving the dispersion in aqueous solutions. Moreover, the combination of graphene and chitosan with $CoFe_2O_4$ nanoparticles is performed to enhance the absorptive properties along with easy magnetic separation of the pesticide from water.⁸ Hence, it is necessary to perform adequate spectroscopy techniques over the sample to obtain the required information for its efficient analysis, including a better understanding of this removal process, in order to point to the real phenomenon regarding its physical or chemical interaction.

The work does not review the adsorption efficiency in a quantitative way, but it is a qualitative work where the interactions between the nanocomposite, its components, and the glyphosate molecule are studied to understand what are the binding mechanisms occurring in the removal process.

Chapter 2 reviews a theoretical background over the nanocomposite compounds along with the spectroscopy techniques working principle used in the study of the nanocomposite-glyphosate interaction being RAMAN, FTIR, and X-ray photoelectron spectroscopy. This is followed by the methodology in Chapter 3 which shows the sample acquisition of the nanocomposite, and the technical specifications of the spectroscopy equipment during the characterization process. Later, a wide analysis and discussion over the obtained results for RAMAN, FTIR, and XPS spectroscopy is performed in Chapter 4 to analyze the molecular and chemical interaction in the removal process. Finally, Chapter 5 can be referred to understand the conclusions obtained from this analysis.

1.1 Problem Statement

There is a need to develop, design, and fabricate eco-friendly and accessible materials for the efficient removal of Glyphosate from water. It has been proved that graphene compounds with chitosan can be used as an adsorption method for glyphosate which can be enhanced when combined with $CoFe_2O_4$.⁸ Therefore, the production of a nanocomposite containing these nanomaterials could be used as an efficient strategy for the remediation of water-containing glyphosate formulations. To show the efficiency of this material, it is necessary to understand the physical and chemical processes happening at the nanoscale. This can be done by performing a set of characterization methods over the samples. Thus, spectroscopy techniques like Raman, FTIR, and X-ray photoelectron spectroscopy might serve as a sufficient study of the molecular interaction in this process.

1.2 General Objectives

Study the adsorption property of a nanocomposite for the remediation of water containing glyphosate pollutants, by performing a detailed analysis of the molecular interaction between graphene, chitosan, and $CoFe_2O_4$ nanocomposite with glyphosate using high energy photon techniques being Raman, FTIR, and X-ray photoelectron spectroscopy to prove its efficiency and reliability of usage.

1.3 Specific Objectives

1. Perform Raman, FTIR, and XPS spectroscopy techniques over the graphene, chitosan, and cobalt ferrite nanoparticles, as well as the nanocomposite before and after interacting with the glyphosate molecule.
2. Analyze and discuss the obtained results in each one of the performed spectroscopy methods to understand the molecular interactions between the nanocomposite, its components, and the glyphosate molecule.

Chapter 2

Theoretical Background

Chemicals-Compounds

2.1 Pesticides

Modern agriculture has a dependency on agrochemicals to maintain the survival rate of the crop and harvest yields.⁵ These agrochemicals are known as pesticides. A pesticide is a mixture of substances or usually biological agents that are released into the environment to avert, control and kill populations of harmful pests. Pesticides are commonly used to kill pests, insects, and other organisms that can attack crops and harm their quality of them. Different kinds have been used for crop protection in the last century. It is widely known that excessive use of pesticides can provoke the destruction of biodiversity.¹⁰ Major classes of pesticides include organochlorines, organophosphates, carbamates, and pyrethroids which are present in the most current and widely used pesticides.¹¹ Generally, the substances present in pesticides are inert contaminants and contain impurities. Being released into the environment these substances break down as metabolites that are toxic to the environment. The risk associated with pesticide use is known to have surpassed its beneficial effects, especially the non-selective pesticides that kill non-target plants and animals, along with the targeted ones.¹²

2.2 Glyphosate

N-(phosphonomethyl)glycerin(glyphosate) is an organophosphorus-efficient broad-spectrum herbicide considered to be the most successful in history applied in agricultural and non-agricultural areas.¹³

The molecule is composed of a fraction of glycine and phosphomethyl being its formula $C_3H_8NO_5P$ as can be observed in Figure 2.1.

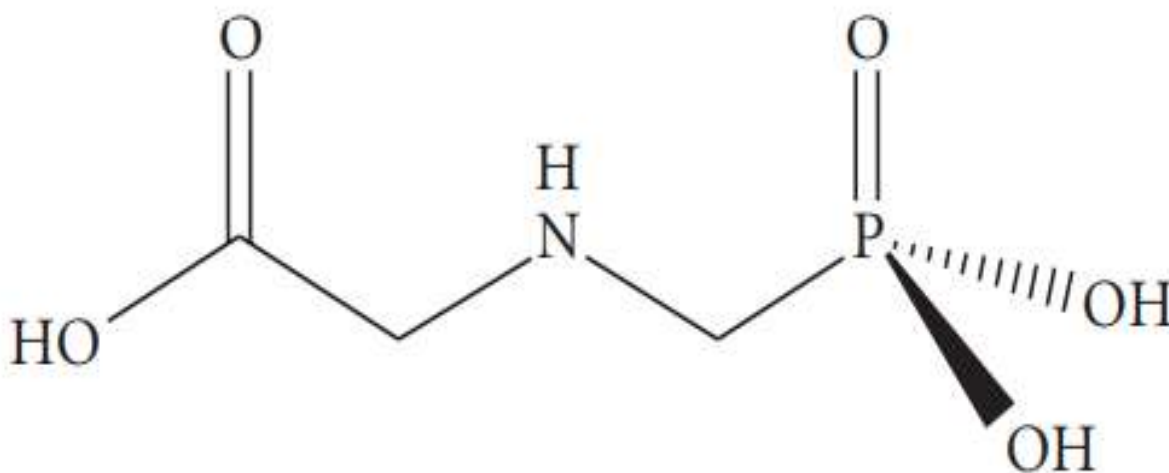


Figure 2.1: Chemical Structure of glycine Glyphosate [N-(phosphonomethyl)].¹⁴

Starting with its first commercialization in the 1970s, glyphosate has become the most used herbicide worldwide with an average usage of about 600 to 750 thousand tonnes annually by 2020.¹⁴

Being a non-selective herbicide, it reduces the growth and activity of nitrogen-fixing bacteria in the soil. It works by the inhibition of some amino acids in plants, fungi, alga, and bacteria. It has been reported to work even on some species of parasites. This pesticide also has harmful effects on earthworms at the cellular level causing DNA damage, and it also affects the activity and viability of some earthworm species.¹⁰ The commercial presentation of glyphosate usually contains not only its main compound but an aqueous mixture of isopropylamine, surfactants, and some other components which can include biocides, and inorganic ions to adjust the pH of the compound, which can vary in concentration and performance. The formulation range from about 41% to 1% glyphosate intended for domestic usage.

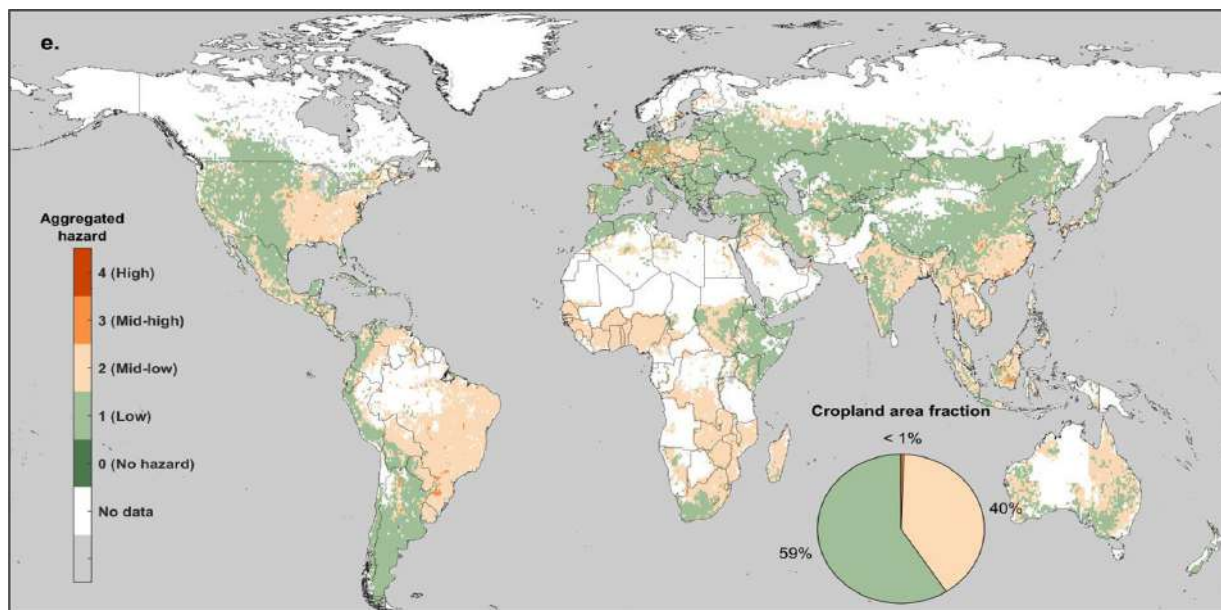


Figure 2.2: Geographic distribution of GLY (Glyphosate) aggregated contamination hazard resulting from biodegradation recalcitrance and residue accumulation.¹⁵

2.2.1 Environmental Impact

Phosphonomethylglycine or PMG as glyphosate is known (also referred to as GLY), degrades in the environment primarily driven by biotic pathways led principally by bacteria and fungi, so its degradation is more appropriate in soil. This substance is very soluble in water contaminating aqueous bodies through various sources like spray drift, spills, or even drainage sometimes unintentional.¹⁶ The concentrations of GLY present in water sometimes exceed $1\mu\text{g}/\text{L}$. When in significant water sources the degradation of glyphosate is considered to be slower, GLY is known to be resistant to hydrolysis in water because of C-N and C-P inert linkages present in the molecule.³ Due to this, the wide usage of glyphosate can lead to serious pollution problems. The geographic distribution of GLY aggregated hazard can be observed in Figure 2.2. Initially, glyphosate should be non-toxic to mammals and birds due to its action mechanisms⁵. On the other hand, fish and invertebrates are more sensitive to the herbicide, especially to its commercial presentation. According to research on commercial glyphosate, its increased toxicity is caused by the surfactants in its composition which cause it to be toxic to non-targeted organisms.¹⁷

2.2.2 Health Issues

A wide number of research on the cancerous effects of glyphosate have been investigated since the early 1990s. The International Agency for Research on Cancer concluded in 2015 that glyphosate is probably carcinogenic to humans, based on evidence in experimental animals and in humans, moreover, it was concluded that strong evidence of genotoxicity and oxidative stress was found in this research.¹⁸

Since January 2001, the northern area of Ecuador has been subject to aerial spraying by the Colombian Government with herbicide formulations that contain glyphosate, and polyethoxylated tallowamine surfactant.¹⁹ The main purpose of spraying glyphosate is to help in eradicating illicit crops in the area. The reason behind using a surfactant in the formulation with is to help the glyphosate in the penetration over the plant knitting causing the compound to be toxic and dangerous to humans.²⁰ In Ecuador, the consequences of aerial spraying with glyphosate added to a surfactant solution have been the main topic in several studies in order to find possible illnesses related to this compound. A study performed over a population in Ecuador showed that a considerable degree of DNA damage was found in an exposed group to glyphosate-surfactant compounds.²¹

2.3 Carbon Nanomaterials

Among materials, carbon-based structures are the most versatile used in the modern field of renewable energy generation and storage as well as in environmental science.²² Among the carbon nanomaterials can be found activated carbon, carbon nanotubes (CNTs), fullerenes, graphene, and graphite. These materials are most widely used in electronic applications due to their desirable properties, both physical and chemical. Among the properties of carbon-based materials, it can be found their low cost, ease of processability, inert electrochemistry, electrocatalytic active sites, and wide surface area among others which are related to the unique atomic structure that the carbon atom possesses.²³ These nanomaterials are arranged as zero-dimensional (fullerenes, and carbon dots), one-dimensional (carbon nanofibers, and carbon nanofibers), two-dimensional (graphene), and three-dimensional (carbon sponges, and graphite) as observed in Figure 2.3.²⁴

2.3.1 Graphene

Graphene is a typical two-dimensional carbon material, consisting of uni-layered graphite consisting of sp²-hybrid carbon as observed in Figure 2.3.²⁵ Graphene is considered to be the basic component of carbon materials in other dimensions which can be conceptually twisted to form fullerenes, rolled into carbon

nanotubes, or stacked in three-dimensional graphite.²⁶ Due to the unique structural features that graphene presents, it owns a variety of intrinsic properties both physical and chemical like high light transmittance, strong mechanical strength, excellent mass, and a large surface area (about $2600 \text{ m}^2 \text{ g}^{-1}$ theoretically).²⁷

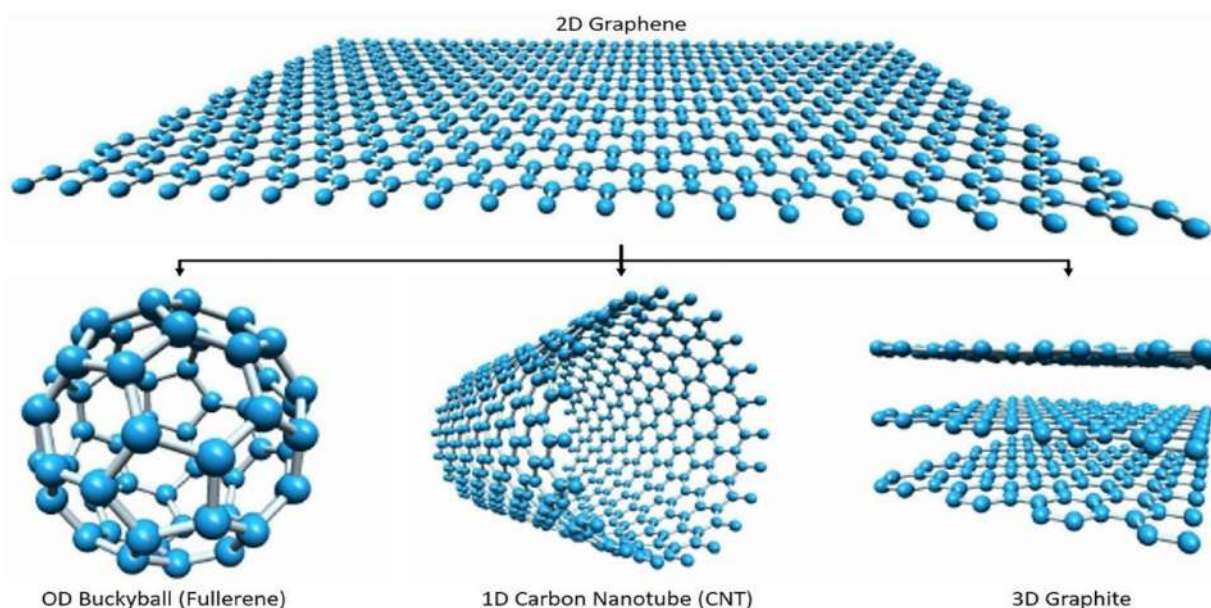


Figure 2.3: Schematic view of graphene 2D structure, 0D fullerenes, 1D carbon nanotubes, and 3D graphite.²⁵

Graphene has several applications in energy storage and conversion, moreover in environmental remediation which is widely studied due to its potential effectiveness.²⁸ There are several different strategies to prepare and obtain graphene, for example, epitaxial growth, liquid-phase exfoliation, zeolite-shear exfoliation, chemical exfoliation, and one of the most used which is chemical vapor deposition (CVD).²⁹ Depending on the method used to obtain graphene it is possible to acquire different pure graphene, or what is usually called graphene derivatives. Due to the high costs related to the synthesis of graphene, graphene oxide (GO) and reduced graphene oxide (rGO) have appeared to be a more economical approach to obtain an efficient alternative to graphene.³⁰

2.3.2 Characterization of Graphene

Characterization of graphene seems to be one of the most important steps of its study and research since it involves the analysis of the present properties, structure, number of layers, and defects of the material based on spectroscopic and microscopic measurements.³¹ The most used characterization techniques when studying graphene include ultraviolet-visible spectroscopy (UV-Vis), scanning and transmission electron microscopy (SEM, TEM), Raman spectroscopy, and X-ray photoelectron spectroscopy (XPS).³² These techniques can provide a whole analysis of the purity and structure of the employed graphene, granting enough information for its possible applications.

2.4 Chitosan

After cellulose, Chitin is the most plentiful natural polysaccharide, which can be mainly found in crustaceans, mollusks, squids, scales of fish, cephalopod beaks, and lissamphibians, as the primary component of cell walls in fungi or even exoskeletons of arthropods.³³ It is a white, inelastic, and hard nitrogenous polysaccharide and the major source of surface pollution in coastal areas, consisting of 2-acetamido-2-deoxy- β -D-glucose through a β (1 \rightarrow 4) linkage which can be degraded by chitinase.³⁴ The structure of Chitin can be observed in Figure 2.4. Chitin is a highly insoluble material that resembles cellulose, because of its solubility and low chemical reactivity. Chitosan is known to be the *N*-deacetylated derivative of chitin.

Considered a modified bio-polymer, it is derived by partial deacetylation of chitin consisting of alternating units of (1 \rightarrow 4) linked glucosamine and *N*-acetyl glucosamine units as shown in Figure 2.4.³⁵ Due to its non-toxicity, antimicrobial properties, and biodegradability, chitosan is used in various applications throughout the biomedical industry, agriculture, genetic engineering, food industry, environmental pollution control, and water treatment.³⁶ Being said this, chitosan can be considered an eco-friendly solution to the pollution caused by the seafood industry since every year almost 80,000 tons of shell waste are produced globally. Conversion of shell waste to chitin and thereafter to chitosan is an effective solution to this problem.³⁷

2.5 Magnetic Nanoparticles

Magnetic materials which are based on metals such as cobalt, nickel, iron, and metal oxides, are involved in different manner of methods in the development of modern technology. These materials can be found

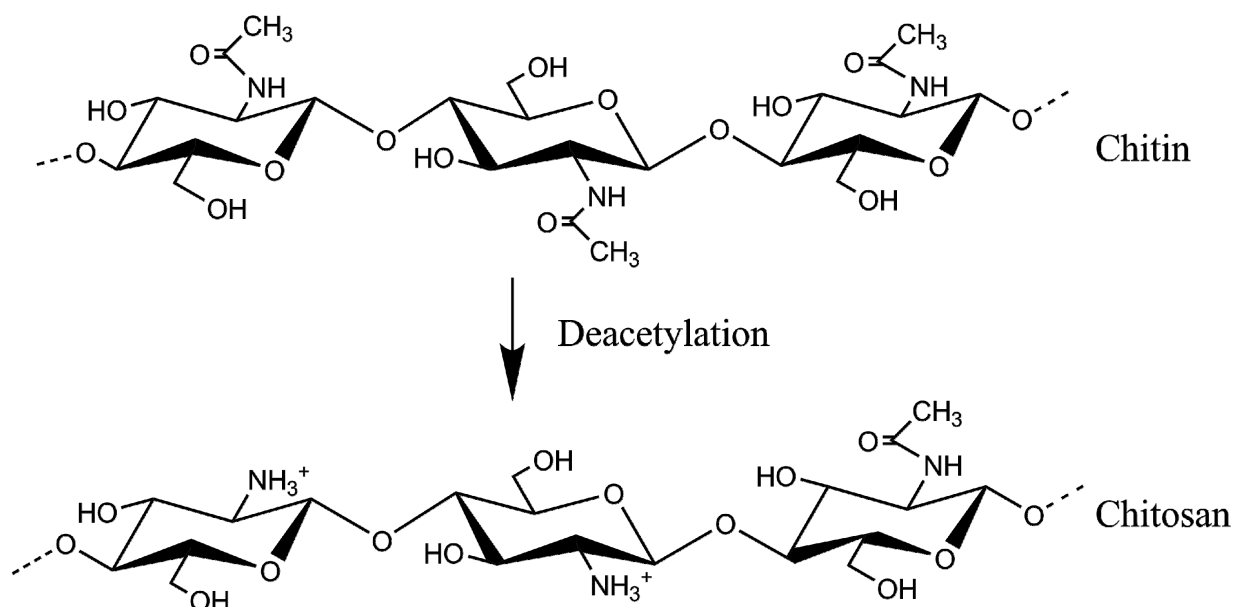


Figure 2.4: Chemical structure of chitin and chitosan (after deacetylation).³⁵

in many devices like motors, sensors, videotapes, and generators, even a computer possesses magnetic materials on its hard disk.³⁸ Whereas nano-structured materials possess unique effects such as electrical, structural, chemical, and magnetic properties, these materials can be used in a variety of novel applications which include information storage, bio-sensing applications, biomedical engineering, and environmental remediation.^{39,40} Being able to understand the magnetic properties of nanometer-scale particles is a known issue in magnetic materials. Consequently, the interest in the nano scaling of these magnetic materials has increased over the last decade since on a very small scale, they can display properties different from the bulk.⁴¹ In most cases, it has been reported that magnetic nanoparticle MNPs smaller than their single domain limit (around 20 nm for FeO_2) can exhibit superparamagnetism even at room temperature.³⁸ Because of the size of the magnetic nanoparticles, they are able to overcome the influence of various forces such as the gravitational field, magnetic field gradient, and the potential magnetic agglomeration which could result when particles come into contact with one another, and they also can be attracted to each other as a result of van der Waals attractive forces (London-type).⁴²

2.5.1 Cobalt Ferrite Nanoparticles

Nanoparticles made of Iron and cobalt can occur in multiple crystal phases. This can result in huge differences in the crystalline anisotropy and magnetic moment due to a possible side effect related to the balance of bulk and surface-free energies for the possible crystal structures depending on the particle size.⁴¹ Iron oxide magnetic nanoparticles containing cobalt have shown improved magnetic properties when compared to only Iron oxide nanoparticles.⁴³ Cobalt Ferrite nanoparticles are a well-known magnetic material with moderate magnetization and a high coercivity making it suitable for various applications.⁴⁴

Cobalt ferrite has a spinel ferrite structure with a characteristic formula MFe_2O_4 , where M can be Co, Ni, Zn, or even other metals. This structure can be described as a closely cubic-packed arrangement of oxygen atoms, M^{2+} , and Fe^{3+} ions which can occupy tetrahedral or octahedral sites.⁴⁵ In the case of cobalt ferrite, the Co ions are in the octahedral sites with an inverse spinel structure where the Fe ions are equally distributed between the tetrahedral and octahedral sites. The molecular structure of cobalt ferrite can be observed in Figure 2.5.⁴⁶

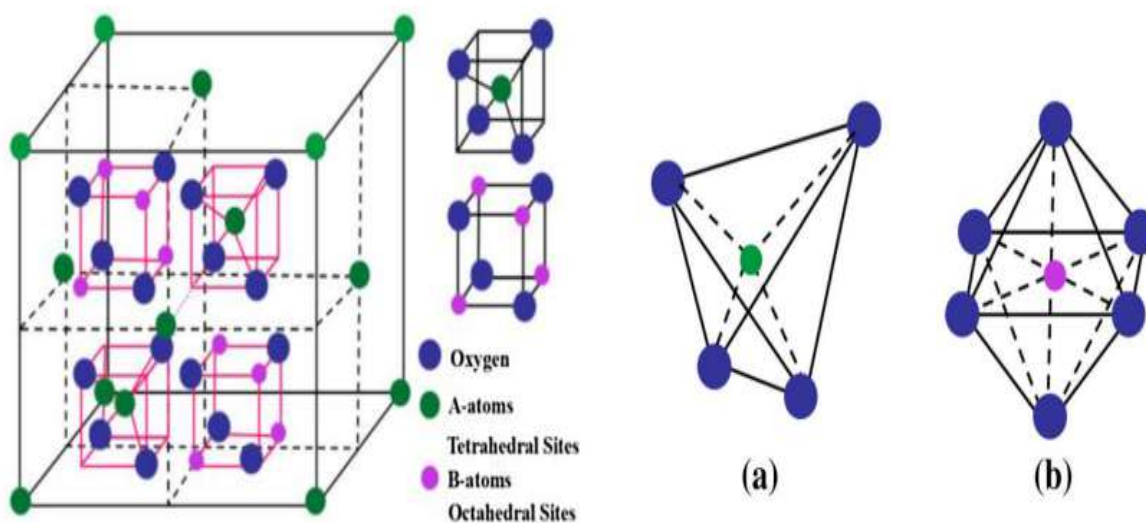


Figure 2.5: Molecular structure of Cobalt Ferrite as it crystallizes in the form of a cubic structure. Each corner of the unit cell consists of a ferrite molecule. a) Tetrahedral sites and b) octahedral sites.⁴⁶

2.6 Nanocomposite

Nanocomposites are the name that receives materials that have a solid structure in which the distance between the bases is leastwise formed of a dimension with nanoscale size. A nanomaterial is generally formed of an organic matrix set in the inorganic phase, or otherwise, from an inorganic phase in the organic phase⁴⁷. Described as amalgamations of varying materials, merged together in nanoscale dimensions, these materials can exhibit individual chemical, electrical, mechanical, and catalytic properties.⁴⁸ Due to the interesting properties that nanocomposites present, the usage of them in diverse fields has increased in the last decade.⁴⁹ Polymeric nanocomposites based on carbon nanomaterials are usually inexpensive with potential for many engineering applications. Some of the studied applications are conductive pastes, supercapacitors, water filters, and pollutant removal.⁴⁷

2.6.1 CoFe₂O₄, Graphene, and Chitosan nanocomposite

The use of graphene and graphene-based nanomaterials provides a greatly viable platform for the production of new types of composites due to the presence of diverse functional groups such as hydroxyl, epoxy, and carboxylic acid.⁵⁰ These groups are important when forming the nanocomposite and various hybrid materials through the simple chemical modification of graphene via organic and inorganic molecules. This also allows covalent and non-covalent chemical functionalization especially performed with polymeric materials enabling the production of graphene-based composite materials with matrix properties and exceptional properties.^{51,52}

In recent studies, graphene-based materials have been used due to their high adsorption capacity together with the low cost that they possess compared to other adsorbents. Theoretically, graphene has a high surface area with good chemical stability, but since it is typically aggregated in aqueous solutions it results in a reduced surface area and decreased adsorption capacity.⁵³ Therefore, it is necessary to form a composite with graphene and other active adsorbents (chemical or physical) that can decrease the aggregation of graphene resulting in an increased adsorption capacity.⁵⁴ Additionally, graphene is known as well to not be easy to recover from the water after the adsorption process. Graphene gains biocompatibility and hydrophilicity when combined with chitosan and can work as a dispersive agent, and as a side effect, it provides non-toxic reactions which are convenient for its use in the environment. As a result, the combination of graphene, chitosan, and CoFe₂O₄ enhances the absorptive properties of the materials alone and allows easy magnetic separation of the nanocomposite from water thanks to the properties that CoFe₂O₄ possesses.⁸

Characterization Techniques

2.7 Raman Spectroscopy

Raman spectroscopy is a non-destructive analytical technique that is commonly used to measure and determine the vibrational energy modes of a sample.⁵⁵ Raman spectroscopy is commonly used in materials science to provide chemical and structural information about a given compound. It also helps in the identification of substances through the so-called Raman "fingerprint".⁵⁶ With this technique, the molecular structure can be examined in detail by analyzing the vibration of its atoms that have a unique position and intensity. These two are affected by the chemical environment factors such as bonds, and forces both inter and intramolecular.⁵⁷

2.7.1 Raman working principle

The electromagnetic field of a photon induces a polarisation of the molecular electron cloud when light is scattered by the molecule. This leaves the molecule in a higher state of energy with the energy of the photon being transferred to the molecule. It is also considered as the formation of a complex between the photon and molecule commonly called the virtual state which is not stable and the photon is remitted immediately as scattered light.⁵⁸ There are three types of scattering processes that can occur when light interacts with a molecule which are Rayleigh scattering, Anti-Stokes Raman scattering, and Stokes Raman scattering as observed in Figure 2.6.

The first scattering occurs when the energy of the molecule is unchanged after it interacts with the photon so the energy and the wavelength of the scattered photon are the same as that of the incident photon. This can also be called elastic scattering and is the dominant process. The Raman scattering which is an inelastic scattering occurs in a much rarer event and it is a process with a transfer of energy between the molecule and the scattered photon. It is called Stokes Raman scattering when the scattered photon loses energy and its wavelength increases. Otherwise, the anti-Stokes Raman scattering occurs when the molecule loses energy by relaxing to a lower vibrational level and hence the scattered photon gains the corresponding energy and its wavelength decreases as observed in Figure 2.6.⁵⁹ From a quantum mechanics point of view Stokes and Anti-Stokes are equally similar processes and considering that in an ensemble of molecules, the majority will be on the ground vibrational level, then Stokes scatter is the statistically more probable process. Then, Stokes Raman scatter will be more intense than its counterpart, and due to this, it is nearly always the scattering process the one measured in Raman spectroscopy.⁵⁶

Raman can be configured in different ways. Being a non-contact technique, it is also possible to use

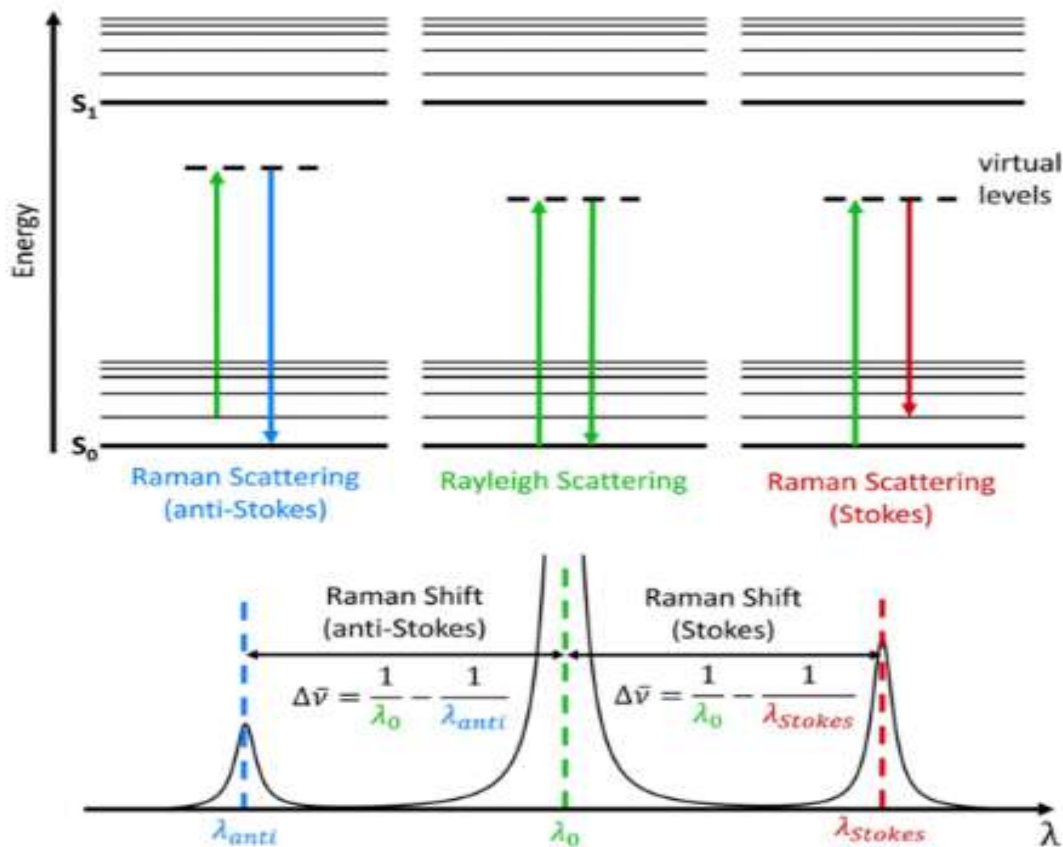


Figure 2.6: Jablonski Diagram showing Rayleigh, Stokes, and Anti-Stokes Raman Scatter.⁵⁹

Raman in an environment with non-clean conditions. Nevertheless, the technique has some limitations considering that it is a weak effect. Due to this, the more common use for Raman spectroscopy is for specific analysis purposes and it can solve many of the standard problems for which it is a suitable technique.⁶⁰ The use of scattering theory is essential to understand the processes behind Raman spectroscopy as well as it is necessary to perform an efficient analysis. Raman spectroscopy has been used to study carbon structures since its discovery. The technique has important applications in graphene-based compounds since it allows the study of its peaks from first to higher-order scattering processes. For all of this, it is considered that Raman spectroscopy has huge potential in the field of nanoscience and nanotechnology.⁶¹

2.8 Fourier Transform Infrared Spectroscopy (FTIR)

Fourier transform infrared spectroscopy also called FTIR is the preferred method used for IR spectroscopy. In this type of spectroscopy infrared radiation is passed through the studied sample where a part of this radiation is absorbed by the sample and the other part passes through. In other words, there is an absorption and transmission process represented in the resulting spectrum as a molecular fingerprint of the sample. Since two fingerprints never match, this makes infrared spectroscopy is useful for several types of analysis when studying different samples in the laboratory.⁶² A spectrum obtained using IR represents the fingerprint of a sample with the absorption peaks corresponding to the frequencies of vibrations between the bonds of the atoms that make up the material.⁶³ Typically an FTIR spectrum is obtained in the range between 400-600 to 4000 cm^{-1} where the spectral bands in the vibrational spectra are specific for a molecule and provide information about the chemical and biochemical composition. These peaks are relatively narrow and can be associated with the vibration of a particular chemical environment or a single functional group present in the molecule.⁶⁴

2.8.1 FTIR working principle

FTIR was developed as a method for measuring all of the IR frequencies of a sample simultaneously by using an interferometer. This interferometer produces a unique type of signal with all of the typical IR frequencies encoded into it and since the signal is measured in seconds, the time element per sample is reduced.⁶⁵ There are three basic components in an FTIR which are the radiation source, the interferometer, and the detector. The job of the interferometer is to divide radiant beams, generate an optical path difference between these beams, and generate interference signals measured as a function of the optical path difference produced by the detector.⁶⁶

The interferometer produces interference signals that contain infrared spectral information which is generated after passing through the studied sample.⁶⁷ The most commonly used interferometer in FTIR is the Michelson interferometer whose basic scheme can be observed in Figure 2.7. This interferometer has three active components which are a moving mirror, a fixed or collimating mirror, and a beam splitter where the radiation of the broadband IR source is collimated and directed into the interferometer and then impinges on the beam splitter to be collected by the detector. Then, the resulting spectrum is produced by decoding the individual frequencies with a technique called Fourier transformation. The transformation is carried out by a computer that presents the user with the resultant spectral information for analysis.⁶⁸

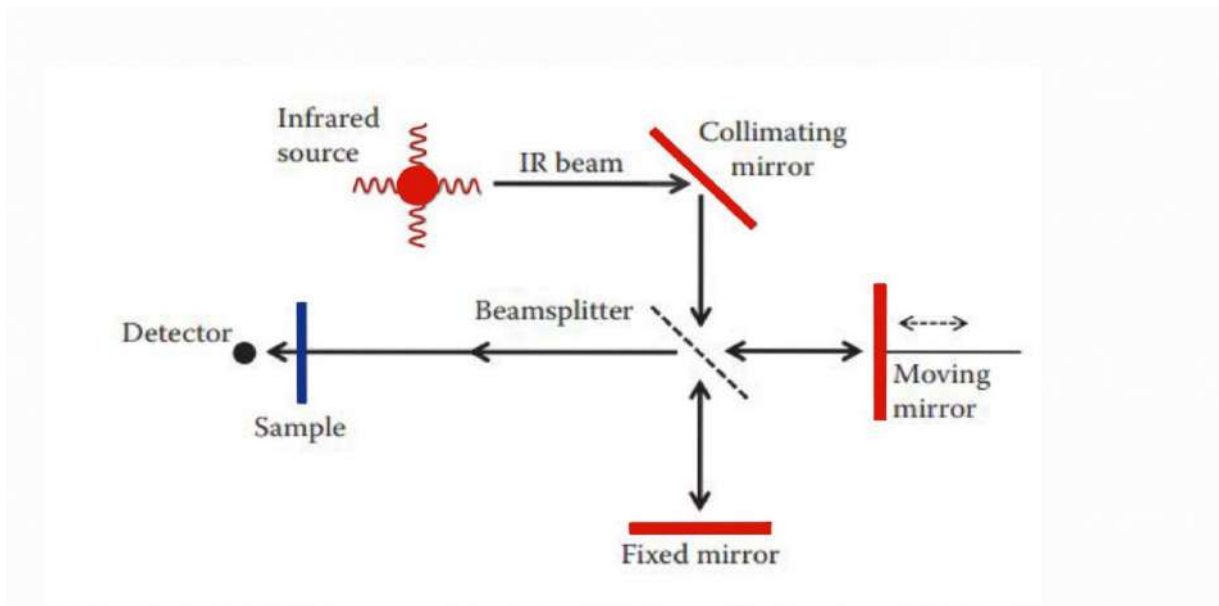


Figure 2.7: Optical diagram of Michelson interferometer where the fixed mirror, the beam splitter, and the moving mirror are observed.⁶⁴

2.9 X-Ray Photoelectron Spectroscopy

X-ray photoelectron spectroscopy, also known as XPS, is a powerful and widely used analytical technique that enables the investigation of the chemical and electronic properties of matter at the surface level. This method is particularly useful for determining the elemental composition, empirical formula, chemical state, and electronic state of the elements present in the sample.⁷⁰ It is a surface-sensitive and quantitative spectroscopic technique that provides a wealth of information on the chemical composition of a material. One of the main advantages of XPS is its ability to study elements within a film and determine what other elements they are bonded to. This information can be obtained by analyzing the peak heights or peak areas of the X-ray photo-electrons emitted from the sample. Additionally, the identification of chemical states can be made from exact measurements of peak positions and separations as well as from certain spectral features. Another advantage of XPS is its high sensitivity and the ability to detect elements in low concentrations, as low as 0.1 atomic percent. This makes it a powerful tool for the characterization of thin films and other samples with minimal sample preparation. Overall, XPS is an essential technique

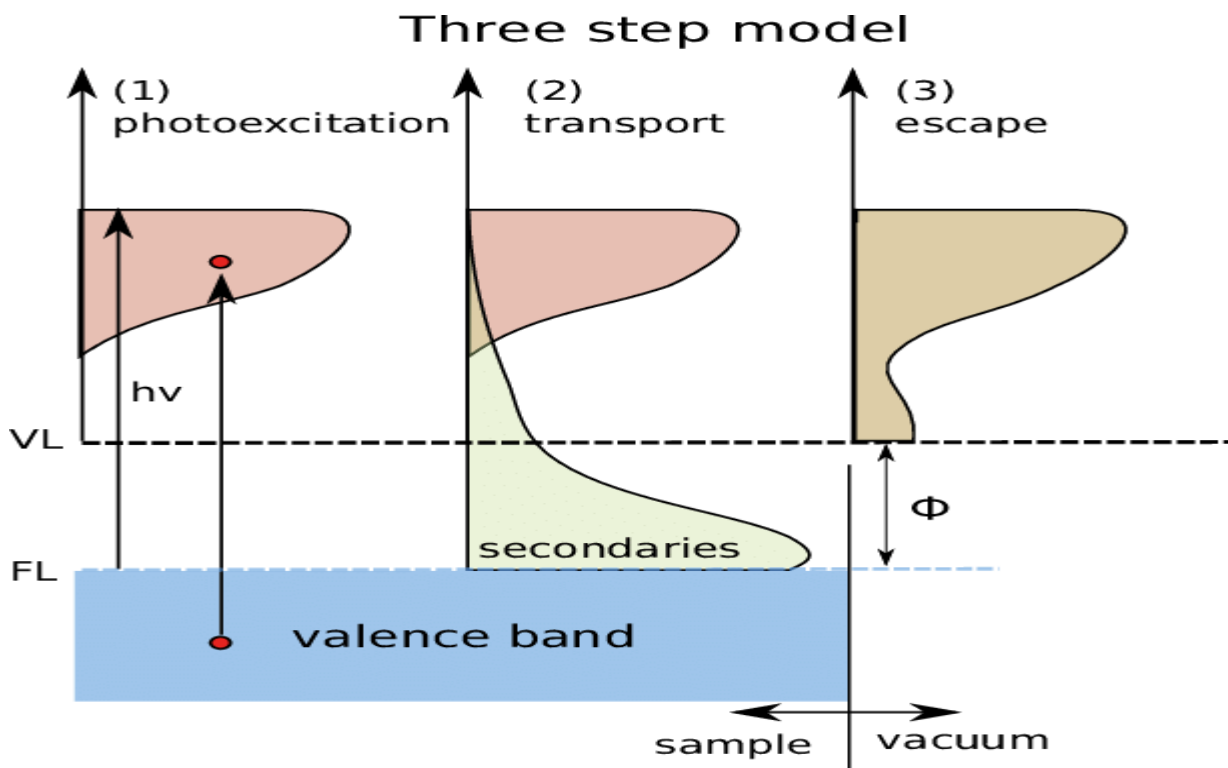


Figure 2.8: Three-step model where the photoemission is divided into 1) photoemission, 2) photoelectron transport to the surface, and 3) photoelectron escape to vacuum.⁶⁹

for the characterization of materials and has a wide range of applications in various fields of science and technology.⁷¹ As XPS is a surface spectroscopic technique, at most the instrument will only explore 10 nm into a sample. Surface analysis of XPS is achieved by exposing a solid sample to a beam of mono-energetic soft X-rays, typically the most used sources are Mg $K\alpha$ (1253.6 eV) and Al $K\alpha$ (1486.6 eV) in a high vacuum environment. The emitted electrons by the photoelectric effect are then analyzed based on their energy.⁷³ The process of XPS typically involves the so-called three steps process which can be observed in Figure 2.8: In the first step, a photon is absorbed by an atom and an electron is excited. This process occurs based on the differential photo-electric cross sections ($d\sigma/d\Omega$). In the second step, the photoelectron travels through the sample to the surface with non-relativistic kinetic energy and is not scattered. In the third step, the electron escapes into the vacuum through the surface energy barrier thanks to the photoelectron kinetic energy which should be higher than the spectrometer work function (ϕ).⁷⁴ The electrons that enter the

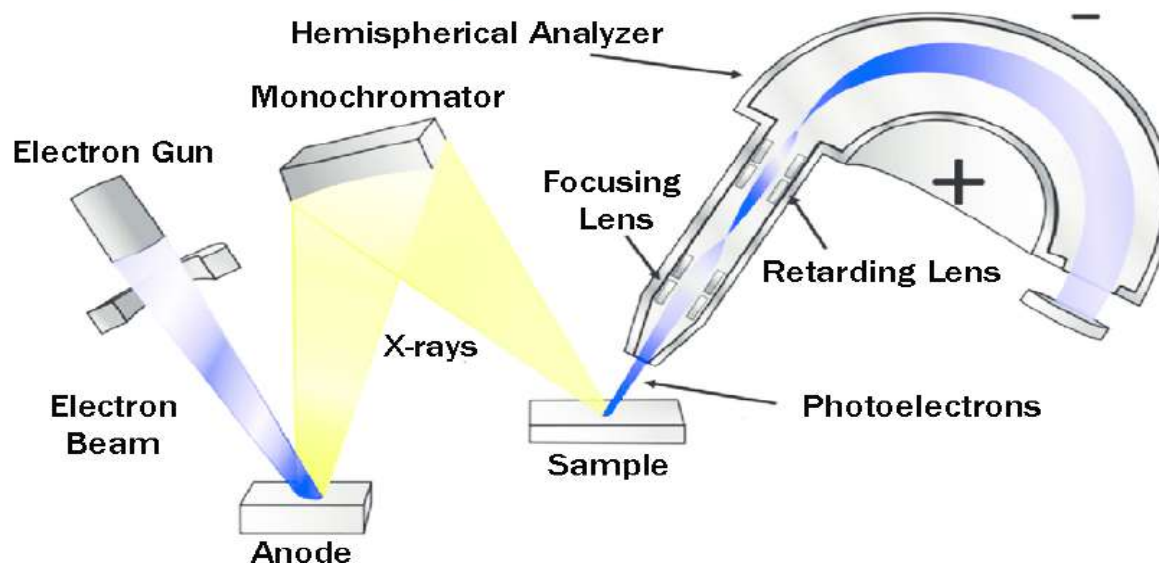


Figure 2.9: Schematic representation of an XPS system showing the electron gun, sample, and the detector.⁷²

collection lens are then analyzed to gain insight into the chemical and electronic properties of the material. The emitted electrons have measured kinetic energies given by the equation:

$$KE = h\nu - (E_B - \phi)$$

Here, $h\nu$ is the energy of the photon and E_B is described as the binding energy of the atomic orbital from which the electron originates. This parameter is the unknown variable that the technique measures and is represented in the obtained result.⁷³ The binding energy may be regarded as the difference between the initial and final states after the photo-electron has left the atom. Because there is a variety of possible final states of ions from each type of atom, there is a corresponding variety of kinetic energies of the emitted electrons. Moreover, there is a different probability or cross-section for each final state. A schematic representation of an XPS system is shown in Figure 2.9.⁷² Here, it is possible to observe the schematic of XPS where fundamentally an electron gun hits the anode, generating X-rays that then go to a monochromator to finally reach the sample's surface. Subsequently, photo-electrons pass through a hemispherical analyzer and then are obtained by the detector to be processed in the computer software.⁷⁵

2.9.1 XPS Data Analysis

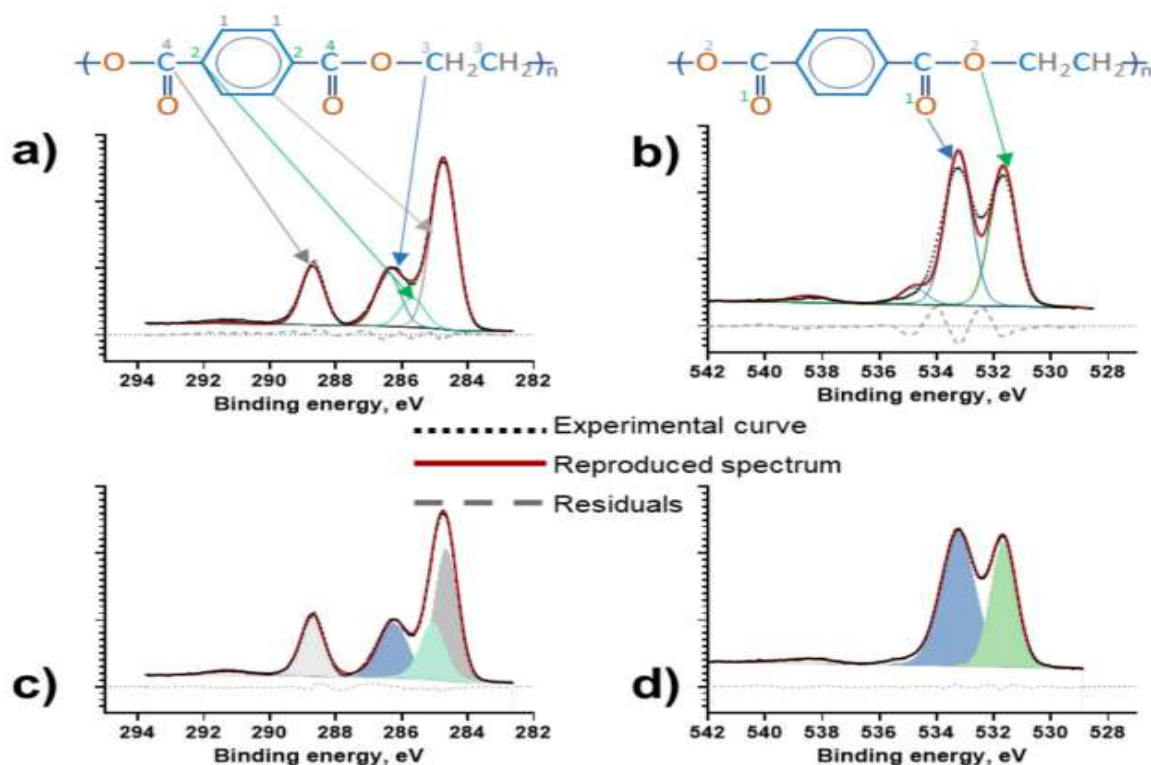


Figure 2.10: High-resolution C1s and O1s spectra fitted using a GLS function with a Shirley background. a) and b) are the initial set of peaks added to fit the curve. c) and d) are the final curve-fitted spectra.⁷⁶

When analyzing XPS spectra, it is convenient to identify two spectral regions which are the core region (electrons with binding energies greater than 30 eV) and the valence band region (BE < 30 eV). In the core region, the spectral features are obtained from photoelectrons coming from the core energy levels called atomic orbitals which are characteristic of the individual atoms in the analyzed sample.⁷⁷ Contrary to this, the features in the valence band region come from photoelectrons generated from energy levels that typically involve the chemical interactions between the atoms in the chemical bonding called molecular orbitals.⁷⁷ The spectra features of core and valence regions are sensitive to the chemical environments of the atoms in a sample, especially in the core region where it is possible to find chemical shifts. These shifts in the binding energies usually yield a series of overlapping peaks when the sample presents atoms in

different chemical environments. Then, one important aspect of the XPS study is treating the XPS spectra where the resulting data can be analyzed by a curve fitting. Curve and peak fitting is usually the only way to extract quantitative information from the obtained spectra.⁷⁸

In an XPS spectrum with a set of component peaks, it is possible to separate the photoemission signal originating from distinct elemental or chemical states. After the process of peak fitting it is possible to know different parameters such as photoemission peak binding energy, the full width at half maximum (FWHM), area, and lineshapes. The position of a peak gives evidence of an elemental or chemical environment assigned to it, and the quantitative information about the concentration of the chemical states is inferred by doing a measurement in the area of each peak corresponding to a component.⁷⁹

2.9.2 Process of XPS spectra fitting

The model for a peak fitting in XPS is determined by the component peaks and a background algorithm. Of these, the peaks are specified using lineshapes corresponding to mathematical functions, and fitting parameters. These parameters permit a component peak to vary in various ways that include position, FWHM, area, Lorentzian, and Gaussian degree character. The component peaks are usually summed and added to the background to form an approximation of the original analyzed data. The expertise in fitting data with peaks lies in selecting the appropriate number of component peaks while making use of proper lineshapes. This is in order to produce peak models capable of measuring physically significant quantities from XPS spectral forms. Then, it is challenging to select the correct physical solution from the set of potential mathematical solutions that in practice is best done by repeating the measurements on comparable samples to verify the performance when analyzing similar materials of known composition. An example of the process can be observed in Figure 2.10.⁷⁶

Usually in this process, the most commonly used mathematical functions are the Gaussian, Lorentzian, Gaussian-Lorentzian sum (GLS), Gaussian-Lorentzian product (GLY), and Voigt functions being the last one a convolution of a Gaussian and a Lorentzian function. Practically, these three functions can be valuable for XPS peak fitting.⁸⁰

Chapter 3

Methodology

This section describes the experimental reagents, preparation of the nanocomposite, and conditions for the experiment. Also here are presented the details of the characterization processes and techniques used to analyze the studied compounds.

3.1 Sample Preparation

The nanocomposite fabrication was not performed but the samples for further spectroscopy analysis were taken from the work done in [Briceño S, C Reinoso. 2022]. However, for a better understanding, here is included a brief description of the methodology of fabrication as observed in Figure 3.1. Starting with the process, 0.1 g of chitosan was dissolved in 100 mL of 2% acetic acid at 80 C with a constant magnetic stirring for 15 min. As well, 0.1 g of graphene was dispersed in 100 mL of 2% acetic acid and was sonicated for 1 h, then reserved in ambient conditions. Then, to prepare the nanocomposite 9 mL of chitosan previously prepared was blended with 1 mL of the obtained graphene. Next, 0.01 g of CoFe_2O_4 nanoparticles were added to the CsGr solution. Finally, the obtained nanocomposite was sonicated for 1.5 h and dried at 60 C for 12 h.⁸ After having obtained the nanocomposite. The removal process was performed by adding 1 mL of the nanocomposite at 100 ppm mixed with 1 mL of glyphosate solution at 250 g/L keeping a room temperature and pH value of 4. The samples of each component of the nanocomposite were put through glyphosate as well to later be measured using Raman, FTIR, and XPS.

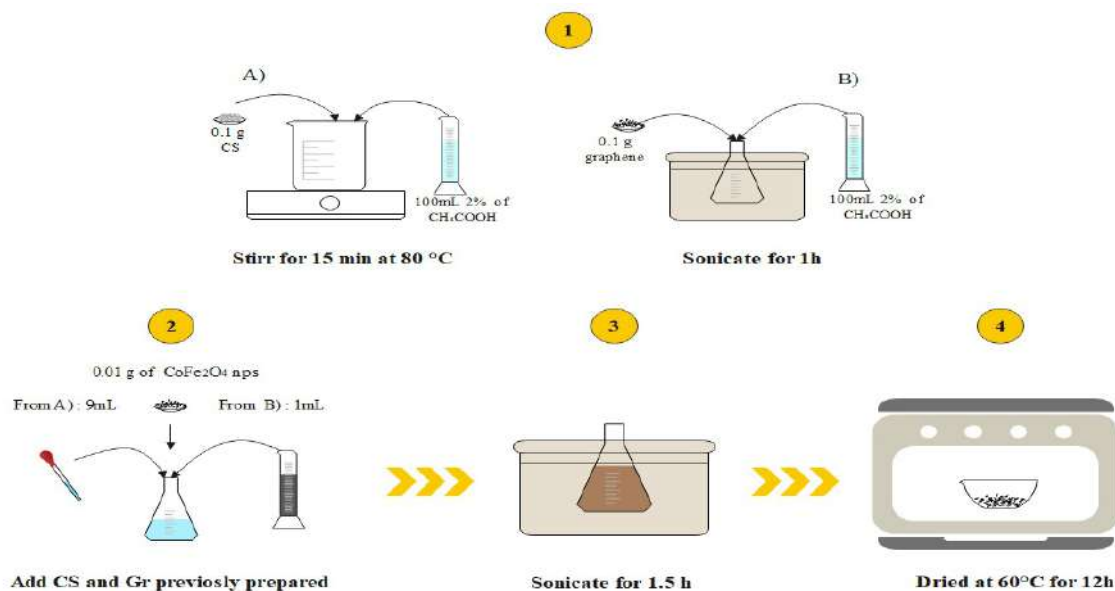


Figure 3.1: Flux diagram of the nanocomposite fabrication.

3.2 Molecular and Structural Characterization

Samples of Graphene (Gr), Chitosan nanoparticles (Cs), Cobalt Ferrite CoFe_2O_3 nanoparticles (Co), the nanocomposite (Nc), along with those exposed to glyphosate (Gly) were characterized using Raman, FTIR, and X-ray photoelectron spectroscopy to have an insight view and understanding of the chemical and physical interactions among them.

3.2.1 Raman Spectroscopy

The Raman spectra were obtained using a HORIBA LabRAM HR Evolution spectrometer located in the Characterization Laboratory at Yachay Tech University as seen in Figure 3.2. To prepare the sample, first, it was dried and powdered, then a thin film of the powder was deposited onto a glass slide. The spectra were collected by exciting the sample with a 532 nm laser wavelength source.

Before acquiring the spectra, it's important to clean and purify the glass slide to prevent any contamination that might affect the results. The thickness of the deposited film can be optimized to maximize the

signal-to-noise ratio and ensure that the sample allows us to have optimal conditions for measurements.



Figure 3.2: Horiba LabRam HR Evolution, Laboratory of characterization Yachay Tech University

3.2.2 Fourier Transform Infrared Spectroscopy

The Fourier Transform Infrared (FTIR) spectra were acquired using a PerkinElmer 1650 spectrometer with the Attenuated Total Reflectance (ATR) mode observed which is observed in Figure 3.3. The spectrometer was set to a spectral range between 4000 and 500 cm^{-1} . The samples were first dried to a powder form to facilitate proper characterization.

Prior to measurement, it's important to thoroughly clean and purify the ATR crystal to avoid any interference in the spectra. The sample should be homogeneously spread on the ATR crystal, ensuring a sufficient amount is deposited to ensure a maximum signal-to-noise ratio. The thickness of the deposited film can be optimized to maximize the signal strength.

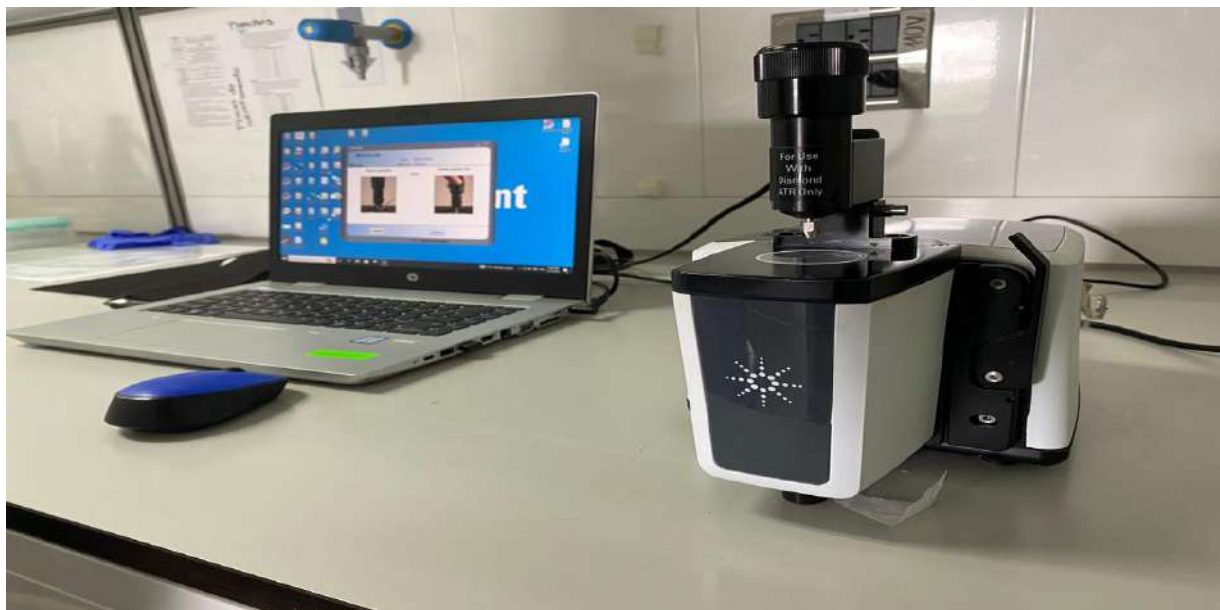


Figure 3.3: PerkinElmer 1650 spectrometer (ATR) mode, Laboratory of characterization Yachay Tech University.

3.2.3 X-ray photoelectron spectroscopy

The X-ray photoelectron spectroscopy (XPS) measurements were carried out using a VersaProbe III 5000 photoelectron spectrometer that can be observed in Figure 3.4. The spectra were obtained using Al K_{α} X-rays with a photon source energy of 1486 eV. The measurements were performed in a high vacuum environment, with a base pressure of 8.10-10 mbar. To achieve this the samples were previously well dried into a powder in order to avoid any liquid component into the XPS chamber as it can prevent reaching the ultra vacuum requirement. Liquid samples were drop-casted onto a silicon wafer and dryer at ambient conditions. Powder samples were placed on a conductive carbon mesh taking precautions of avoiding fractures in the surface in order to bypass possible information from the carbon tape.

A survey scan was first collected for each sample, covering a spectral range of 0 to 1100 eV with a pass energy of 226 eV. This was followed by high-resolution scans with an energy band pass of 55eV in specific regions for different elements of interest, such as C1s, N1s, O1s, P2p, and S2p for Gr, Ch, Gly, and C1s, O1s, Fe2p, and Co2p for Co. The high-resolution scans were repeated several times (between 10 to 20 times) to increase the signal-to-noise ratio and improve the data according to the intensity of the

peaks in the survey scan.

To avoid electrostatic charging of the sample, an electron flood gun was used during the measurement. The binding energies were referenced to the C1s adventitious carbon peak located at 284.8 eV, and the Au main band at 84 eV was used to calibrate the charge effect in the obtained spectra. It's important to ensure that the spectrometer is properly calibrated and that the X-ray source energy, pass energy, and electron flood gun settings are optimized for the sample being studied.

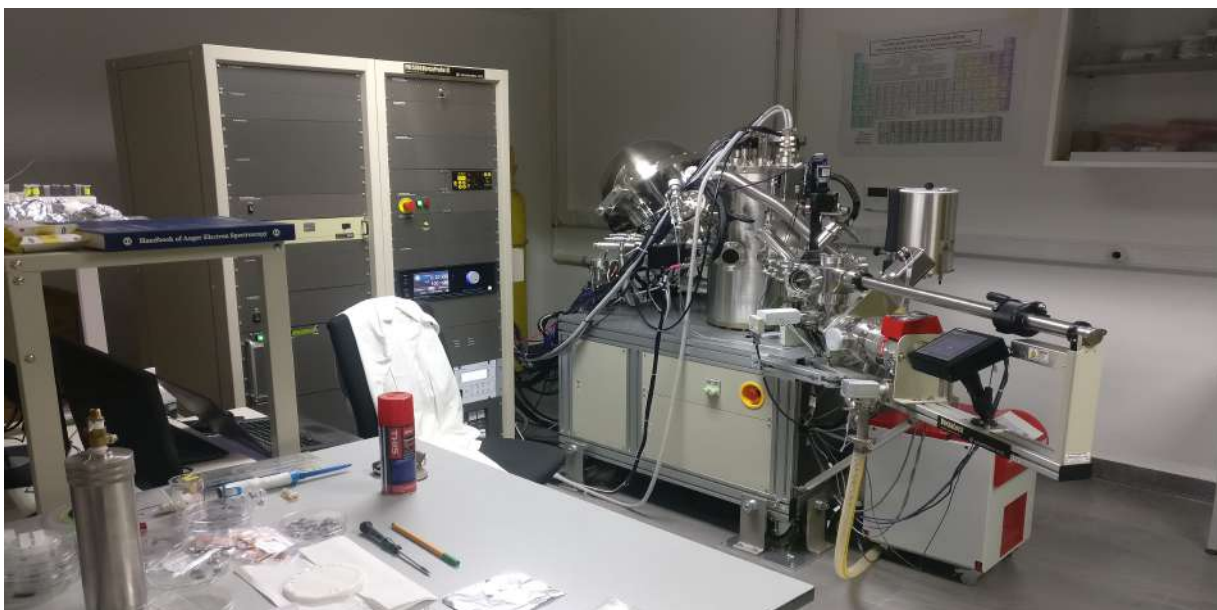


Figure 3.4: XPS Versaprobe III 5000 located in the Laboratory of Characterization at Yachay Tech University

XPS Data Treatment

The data analysis was carried out using Origin Pro, and MultiPak software with a student license. The mathematical function used to perform the peak fitting of the High-resolution spectra were Gaussian, Lorentzian, and Voigt functions along with Shirley and Tougaard backgrounds chosen as they were required. This was done in order to obtain the different peak-line components of each spectrum. In XPS, natural line shapes are assumed to be Lorentzian. However, this line shape is not observed experimentally. This

is caused by the excitation of photo-electrons that travel through a spectrometer broadening the signals to some degree.⁸⁰

During the peak fitting process is important to notice that the background is not subtracted since it can lead to the loss of information. In the technique of peak fitting an XPS high-resolution scan, generally, one selects a baseline first followed by a series of peaks called synthetic fit components. As mentioned before, in this work we chose The Gaussian, Lorentzian, and Voigt functions which are the most common. In equations 3.1 and 3.2 can be observed the Gaussian and Lorentzian mathematical functions respectively.⁸¹

$$G(x; F, E, h) = h \cdot \exp \left[-4 \ln 2 \frac{(x - E)^2}{F^2} \right] \quad (3.1)$$

$$L(x : F, E, h) = \frac{h}{\left[1 + 4 \frac{(x-E)^2}{F^2} \right]} \quad (3.2)$$

Using both software, in Origin Pro, a better approach was obtained using Gaussian and Lorentzian functions while in MultiPak the software automatically used Voigt functions as a convenience. In general, for the Peak fitting of C1s, O1s, N1s, and P2p a Tougard baseline was employed, and for Co2p and Fe2p a Shirley baseline was utilized.

Chapter 4

Results & Discussion

Characterization of Materials

Information on the physical, chemical, and morphological properties of the samples is obtained through characterization techniques. The obtained results will be related to the interaction of the glyphosate molecule with the components of the nanocomposite. This Chapter describes the characterization of the obtained samples to obtain the required information on chemical composition, bonding interactions, and binding energies present in the compounds. In order to achieve this, the used spectroscopy techniques were Raman spectroscopy, Fourier transforms spectroscopy (FTIR), and to provide a better understatement of the molecular interactions, X-ray photoelectron spectroscopy (XPS).

4.1 Raman Spectroscopy

The Raman spectrum was obtained for the chitosan, graphene, cobalt ferrite nanoparticles, nanocomposite, and glyphosate. Figure 4.1(a) shows the Raman spectra for graphene, it is observed that the broadening effect increases of the spectrum increase when the glyphosate (250 g/L) interacts with the formed magnetic nanocomposite (Gly-Nc). The Raman spectrum for glyphosate is observed in Figure 4.1(b), here are observed the peaks assigned to P-O, C-H, and -CH₂. The three compounds are joined together to form the nanocomposite (Nc) where the Raman spectrum can be observed in Figure 4.1(c) showing a broadening of the D and G peaks of graphene. This is due to the lattice strain stemming from the interaction between the Gr sheets, and the cobalt ferrite nanoparticles. In Figure 4.1(d) is observed the Raman spectrum of the CoFe₂O₄ nanoparticles where can be observed two main peaks at 2912 cm⁻¹ and 1461 cm⁻¹ which

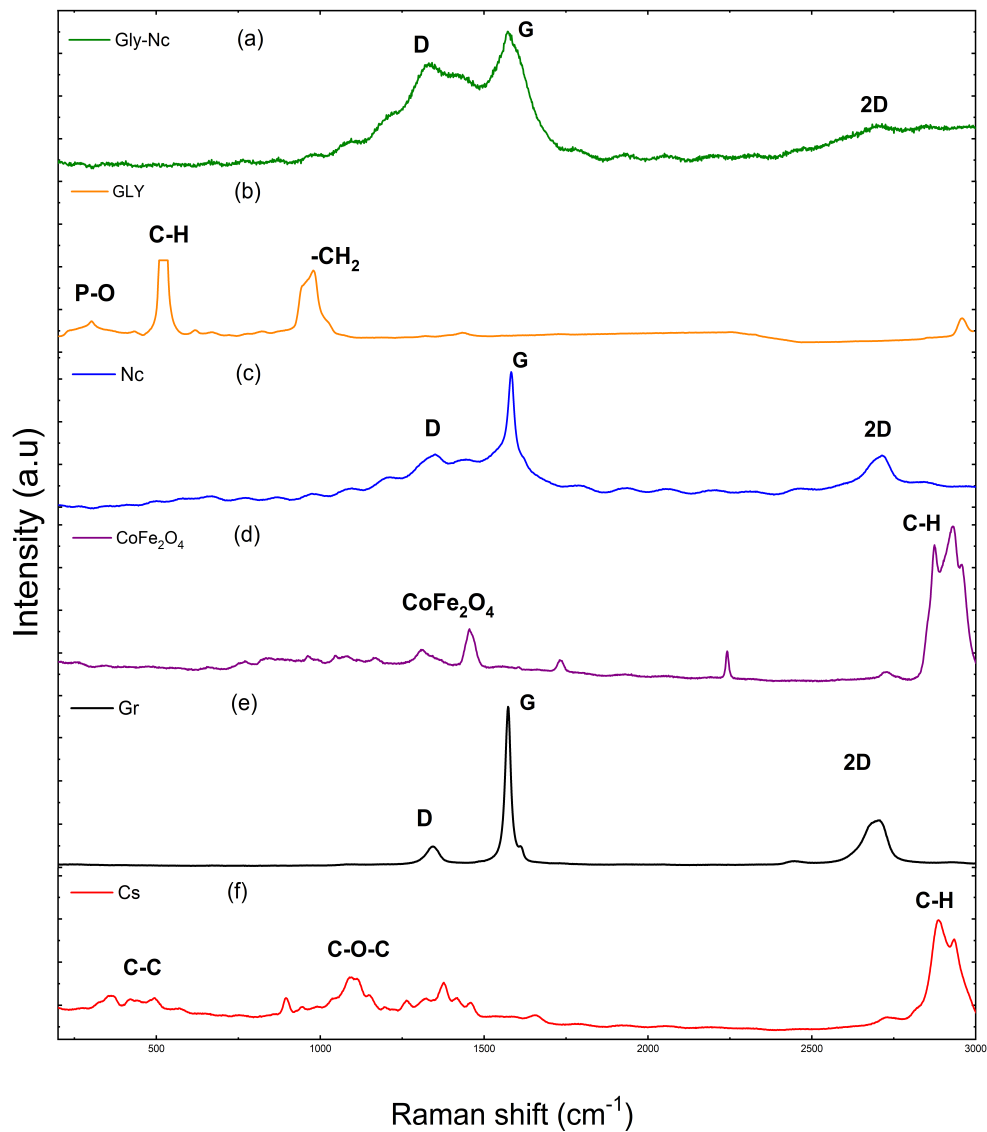


Figure 4.1: Raman spectrum of (a) glyphosate-nanocomposite (Gly-Nc), (b) glyphosate (Gly), (c) nanocomposite (Nc), (d) CoFe₂O₄ nanoparticles (Co), (e) graphene (Gr), and (f) chitosan (Cs) obtained with an excitation laser of 532nm.

are a C-H bonding and the characteristic peak of cobalt ferrite respectively. Also, the Raman spectrum of commercial Graphene is observed in Figure 4.1(e) which is structured by the D, G, and 2D peaks at 1335 cm^{-1} , 1589 cm^{-1} , and 2705 cm^{-1} which is characteristic of graphene. The Raman spectrum Chitosan is shown in Figure 4.1(f) where can be observed three main peaks. The first peak represents a C-H bonding and is located at 2912 cm^{-1} , the second one represents a C-O-C bonding (ether) at 1100 cm^{-1} , and the third corresponds to a P-O bonding found at 500 cm^{-1} . Refer to Table 4.1 to see a complete assignment for each peak in the plot.⁸²⁻⁸⁶

Table 4.1: Raman shifts of chitosan (Cs), graphene (Gr), CoFe_2O_4 nanoparticles (Co), nanocomposite (Nc), glyphosate (Gly), and glyphosate-nanocomposite (Gly-Nc).

Raman Shifts (cm^{-1})						Assignment
Chitosan	Graphene	CoFe_2O_4	Nc	Gly	Gly-Nc	
2912		2912				C-H ⁸⁷
	2705		2705		2698	2D-mode ⁸²
	1564		1589		1589	G-mode ⁸³
		1461	1446		1446	CoFe_2O_4 ⁸⁴
	1335		1335		1335	D-mode ⁸³
1100						C-O-C ⁸⁸
				970		-CH ₂ ⁸⁵
				520		C-H ⁸⁵
500						C-C
				300		P-O ⁸⁶

Additionally, It is remarkable to perform further analysis of the interaction between each one of the components of the nanocomposite with glyphosate. Figure 4.2 a) shows the interaction between glyphosate-graphene where in the resulting Raman spectra, it can be observed that the most contribution comes from glyphosate while the peak corresponding to -CH₂ decreases. In Figure 4.2 b) is observed as well, the interaction glyphosate-chitosan where the resulting spectra show the peak corresponding to C-H and -CH₂ groups while the P-O peak is not present. In Figure 4.2 c) the interaction glyphosate- CoFe_2O_4 shows a similar behavior where the peaks for P-O, C-H, and -CH₂ remain, and also there exist some peaks around 1500 cm^{-1} that corresponds to the CoFe_2O_4 . Finally in Figure 4.2 d) is plotted the Raman spectrum obtained from the interaction glyphosate-nanocomposite. This section is interesting since it observed that the resulting Raman spectrum for Gly-Nc is very similar to the Nc spectrum where the peaks found in Gly

are not evidently visible. In all the cases, some of the peaks corresponding to the glyphosate spectrum fade or reduce their intensity. The observed results can be due to some chemical binding interaction between the glyphosate molecule and each one of the components of the nanocomposite which will be determined in a more suitable manner using FTIR, and XPS.

4.2 Fourier Transform Infrared Spectroscopy (FTIR)

The FTIR spectrum obtained for the interaction between the nanocomposite, each one of its components, and the glyphosate molecule is observed in Figure 4.3. Moreover, for each spectrum are displayed two main regions, the first being called the Functional group region from 1500 cm^{-1} to 3900 cm^{-1} , and the second one called the Fingerprint region which is located from around 390 cm^{-1} to 1500 cm^{-1} as observed in Figure 4.3. In the functional group region, it is identified in the Gly-Gr the sp^3 C-H stretching vibrational mode which is not present in any other of the interactions with the glyphosate molecule. Notice that the sp and sp^2 C-H stretchings are not present over 3000 cm^{-1} . Around 2000 cm^{-1} are observed the aromatic overtones (or aromatic rings), marked with a square in Figure 4.3. These aromatic rings are primarily present in most organic materials.^{89,90} About 1700 cm^{-1} is found a scissoring bending, N-H bend (potential amines, amides) together with C=O and C=C groups. Between 1350 to 1000 cm^{-1} is found a C-O stretching and Below 1000 cm^{-1} corresponds to a carbon isomer. In Figure 4.3 it is observed around 1050 cm^{-1} a square which marks the phosphate group present in the glyphosate.^{86,91-96}

Figure 4.4 shows the interaction between glyphosate and the components forming the nanocomposite through a zoom in the Fingerprint region between 450 cm^{-1} and 1500 cm^{-1} . There are some remarkable aspects found in this region. First, the characteristic vibrations of the carboxylic and amino groups due to the N-H scissoring and bending vibrations near 1650 cm^{-1} can be located in the range from 1800 cm^{-1} to 1300 cm^{-1} . Here, is observed a decrease in the intensity of the C-H deformation vibration from -N-CH₂- and the C-N stretching vibration near 1370 cm^{-1} and 1320 cm^{-1} respectively. This suggests an interaction between the glyphosate and the nanocomposite surface. Then, in the range from 1300 cm^{-1} to 850 cm^{-1} are located the bands related to the changes in the composition of the phosphonic group. In this section, it can be identified the components of the phosphate present in the glyphosate molecule which are the P-H, P-OH, P=O, and PO₂ groups. It is noticeable that some of these bands become sharpen while others reduce their intensity or shift as is the case for the peak belonging to P-H, and P-OH. This is when interacting the nanocomposite with the glyphosate (Gly-Nc) in Figure 4.4 which demonstrates the strong interaction of glyphosate with the metal ions of the nanoparticles potentially due to the coordination of the cobalt and iron thanks to the phosphonic carboxylic groups. Furthermore, when analyzing the Gly-Nc with glyphosate, the

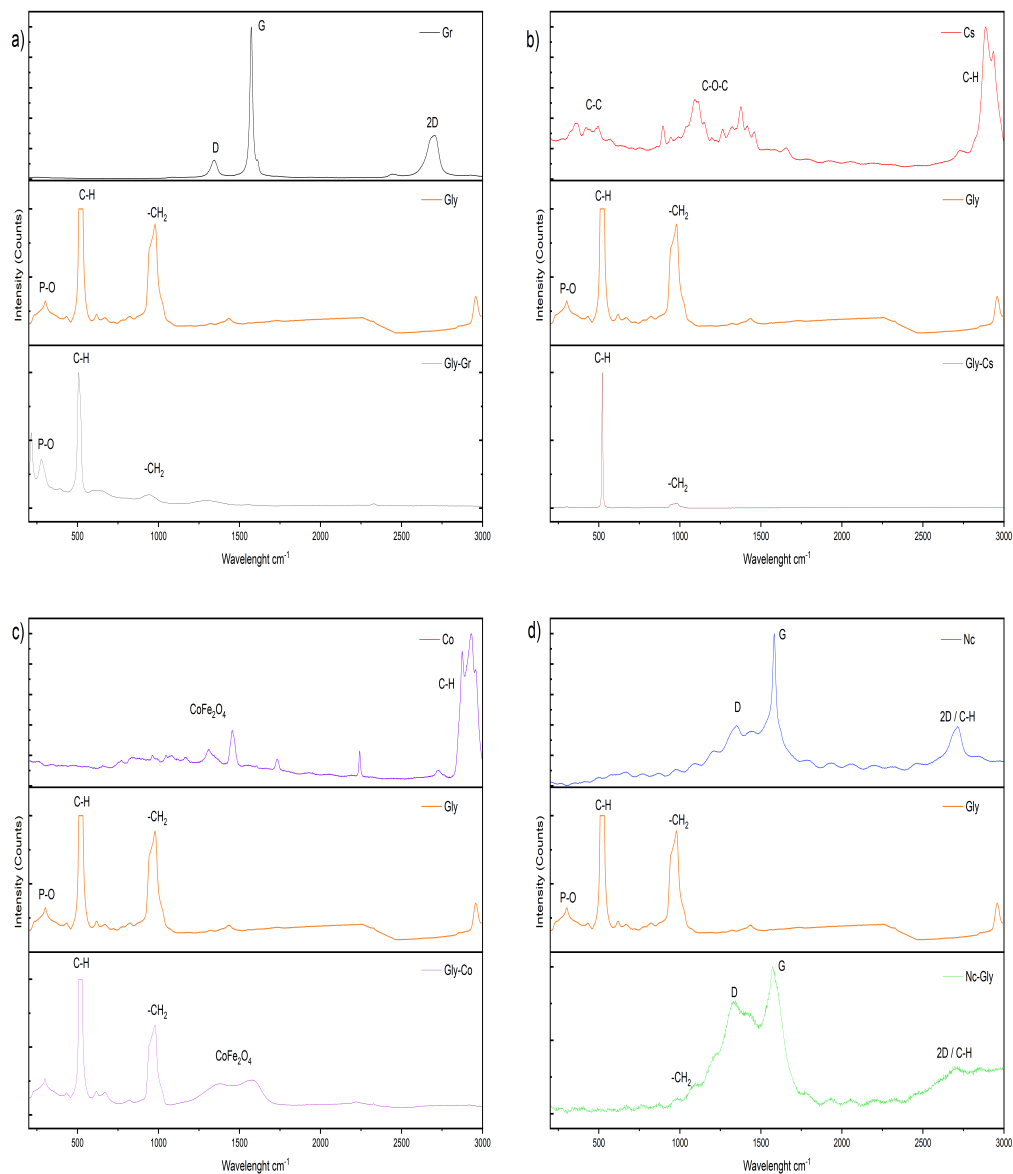


Figure 4.2: Raman spectrum for the interactions Gly-Gr a), Gly-Cs b), Gly-Co c), and Gly-Nc d).

peaks belonging to the phosphate group PO_2 in the glyphosate spectrum around 1070 cm^{-1} are still present with a strong signal but with a sharpened peak in comparison to the sole interaction Gly-Gr, Gly-Co, and

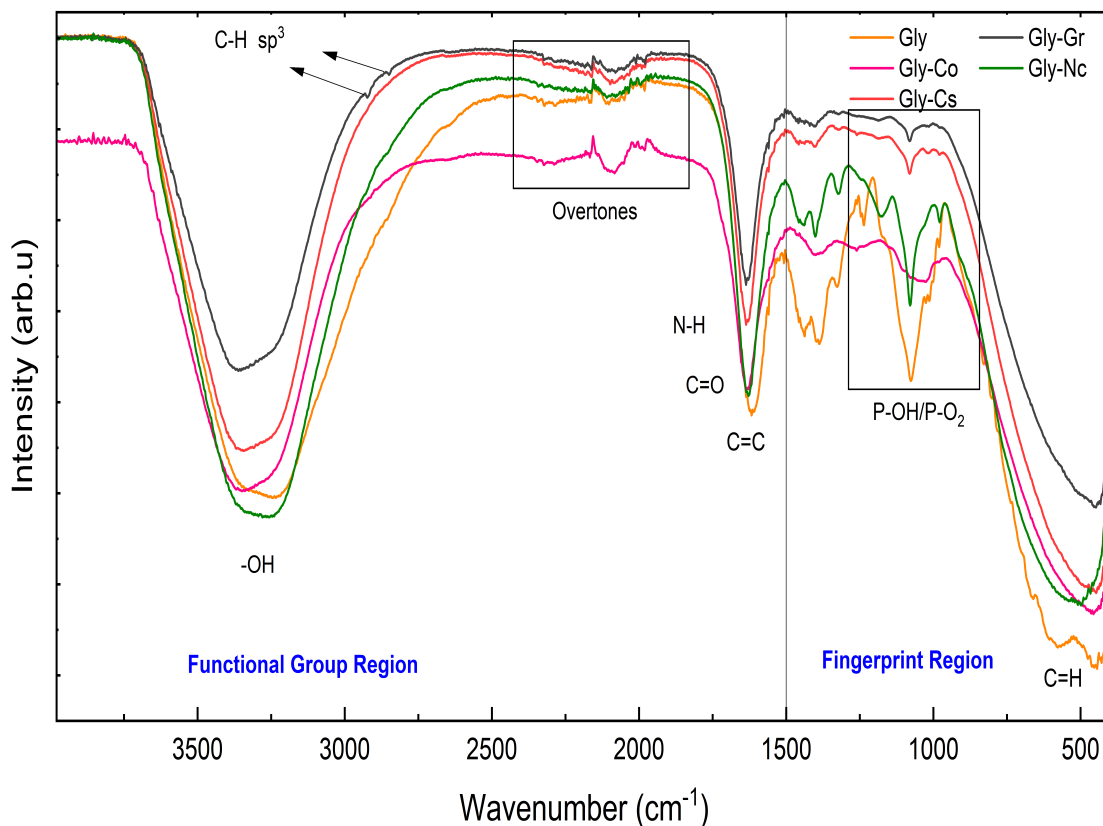


Figure 4.3: Fingerprint Region from 850 cm^{-1} to 1800 cm^{-1} of glyphosate and the interaction between glyphosate with graphene, chitosan, cobalt ferrite nanoparticles and the nanocomposite (Gly, Gly-Gr, Gly-Cs, Gly-Co, Gly-Nc).

Gly-Cs where they aren't almost present. This shows that indeed there is an interaction between glyphosate and the nanocomposite through this functional group likely due to a direct interaction occurring through the phosphate group present at the glyphosate and iron ions of the nanocomposite. In addition to this, is easy to identify the N-O peak around 980 cm^{-1} belonging to nitrogen compound reassuring the presence of surfactants (additives) used in the commercial formulation for glyphosate.^{86,91-97}

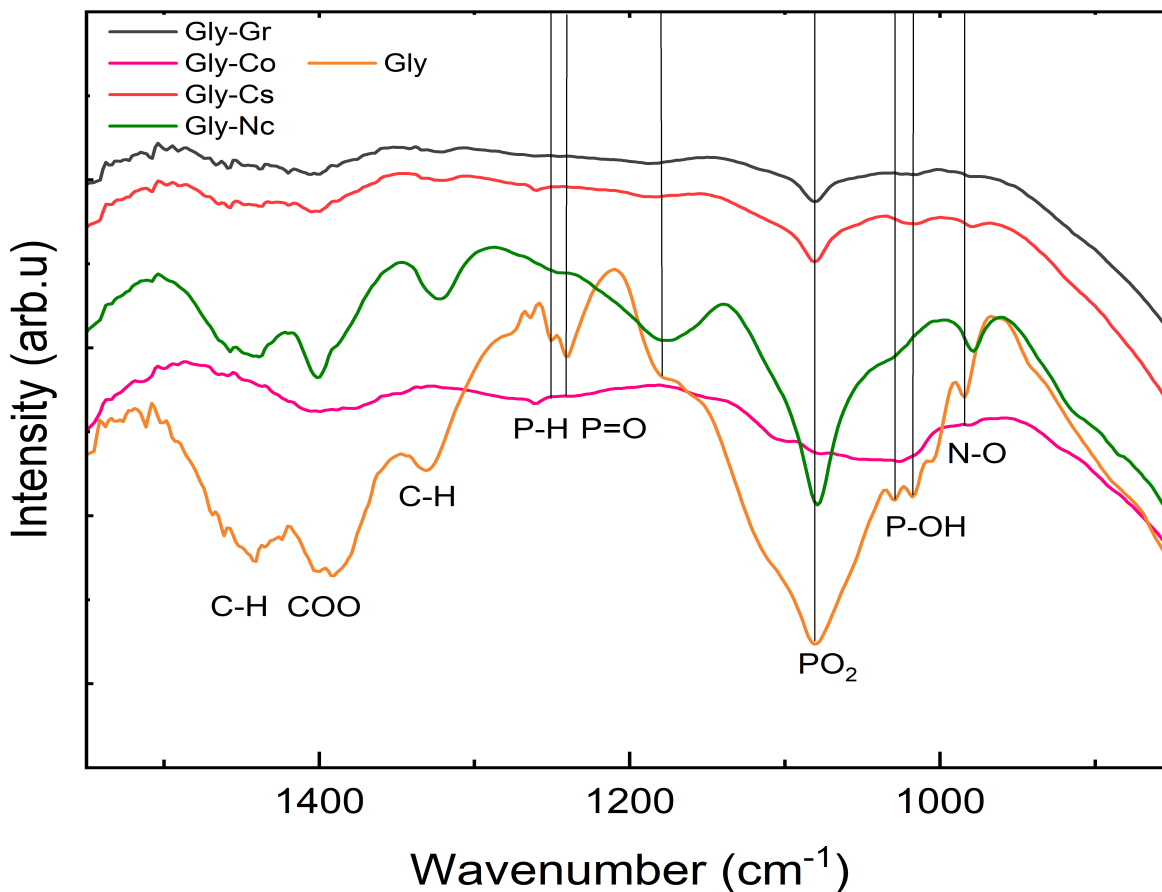


Figure 4.4: Fingerprint Region from 850 cm⁻¹ to 1500 cm⁻¹ of glyphosate and the interaction between glyphosate with graphene, chitosan, cobalt ferrite nanoparticles and the nanocomposite (Gly, Gly-Gr, Gly-Cs, Gly-Co, Gly-Nc).

4.3 X-ray Photoelectron Spectroscopy (XPS)

In this section, X-ray photoelectron spectroscopy was utilized to measure the atomic concentrations and binding energies belonging to the functional groups located at the surface of the magnetic nanocomposite. The XPS measurements were performed in the region from 0 to 1400 eV. This was performed before and after the glyphosate adsorption for graphene, chitosan, cobalt ferrite, and the nanocomposite.

4.3.1 Interaction Glyphosate-Graphene (Gly-Gr)

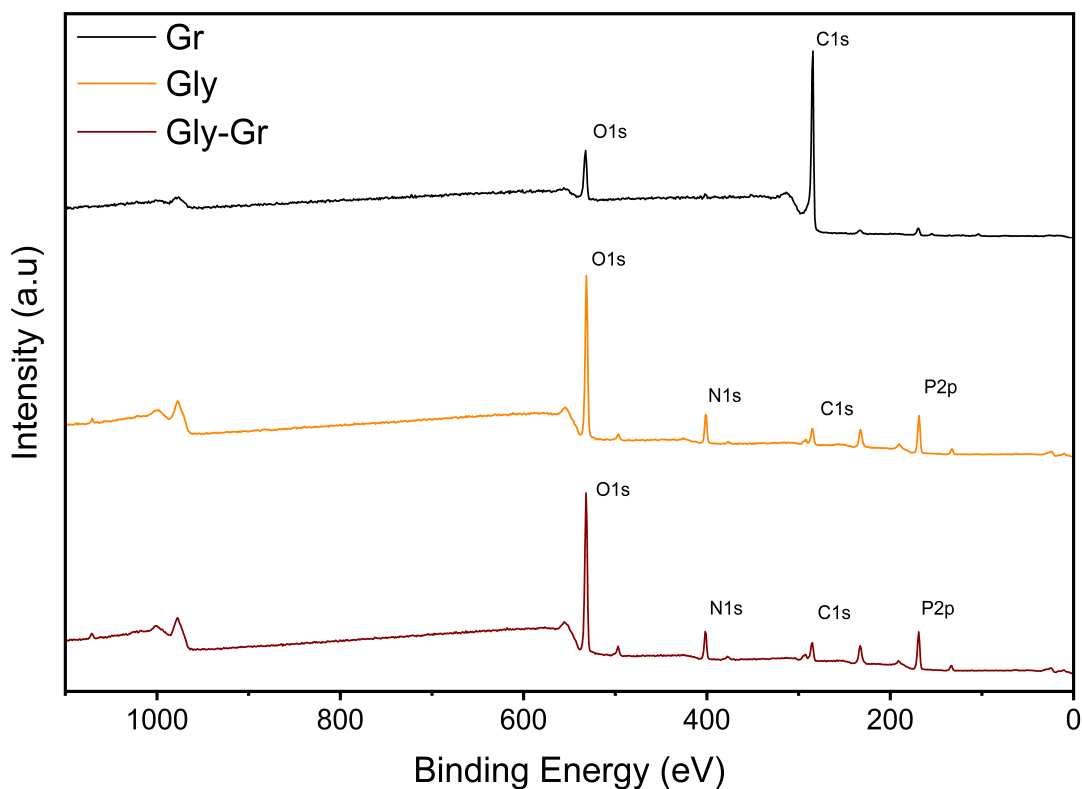


Figure 4.5: X-ray photoelectron survey spectrum of glyphosate (Gly), glyphosate-graphene (Gly-Gr), and graphene (Gr).

An XPS analysis was performed to understand the interaction between glyphosate (Gly) and graphene (Gr) before and after the absorption of this compound. In Figure 4.5 is easily noticeable the XPS survey spectra for graphene, glyphosate, and the interaction between the two respectively. In the figure is observed in the first instance that there is a predominant presence of oxygen O1s, carbon C1s, nitrogen N1s, and phosphorus P2p which were studied through a high-resolution measurement.

By looking at Figure 4.6 i), it is shown a great contribution of carbon C1s thanks to the vast amount

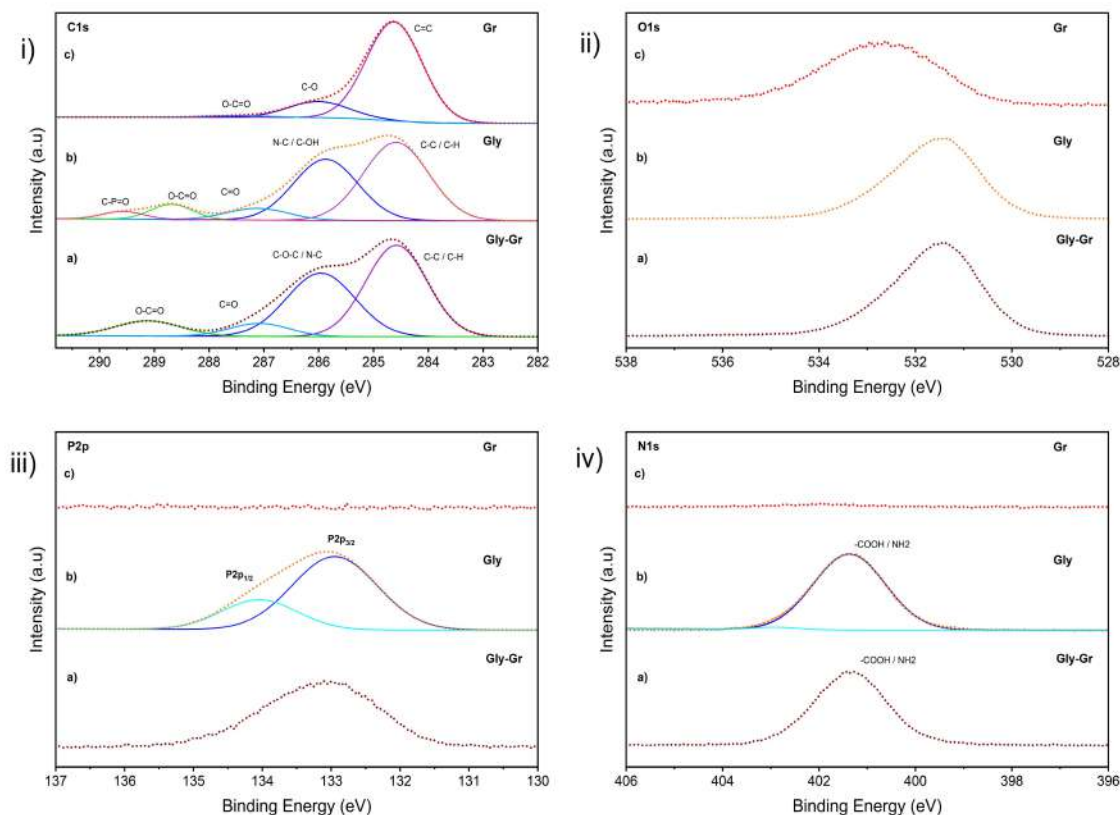


Figure 4.6: X-ray photoelectron high-resolution spectrum of glyphosate (Gly) a), glyphosate-graphene (Gly-Gr) b), and graphene (Gr) c) in the areas of carbon C1s i), oxygen O1s ii), phosphorus P2p iii), and nitrogen N1s iv).

of functional groups in the molecules, this is inferred due to the big with at half maximum value number which shows the presence of different bindings. in the C1s spectra, there is no evident shift between the binding energies but a difference in areas due to the increment of the bonding which can be understood as a bigger interaction in this area. In Table 4.2 we can observe the difference in the areas for the C1s binding energies. First, we have the C-C/C-H bonding located around 284.6 eV. Here, is feasible to observe that the percentage compared to Gly in Gly-Gr increases. Something similar occurs for the binding energy around

286 eV which corresponds to the N-C, C-OH, and C-O-C bindings. In this part, the atomic concentration increases as well showing an interaction in this area. This can be comprehended as an effective relationship in the C1s zone due to the presence of the carboxyl, amine, and phosphate groups.⁸⁶

Table 4.2: C1s atomic concentrations of Graphene (Gr), glyphosate (Gly), and graphene-glyphosate (Gly-Gr)

C1s Binding-Energies Atomic Concentration (%)			
Graphene (Gr)	Glyphosate (Gly)	Graphene-Glyphosate (Gly-Gr)	Assignment
83.67	47.67	48.11	C=C / C-C / C-H
14.81	36.75	37.05	O / N-C / C-OH / C-O-C
1.50	6.70	6.47	C-C=O
	5.90	8.35	O-C=O
	2.95		C-P=O

The interaction in the Oxygen O1s area is observed in Figure 4.6 ii) where it can be observed there it don't exist an increment in the full width at half maximum value comparing Gly and Gr-Gly after the glyphosate absorption, but a decrease compared to the sole graphene. This may be caused because of the interaction of oxygen functional groups in the adsorption process observed in the C1s spectra as well, where the oxygen groups are lesser in the Gly-Gr compound than in Gr. This is also inferred from the shift that exists between the Gr spectrum and the Gly-Gr. The interaction in the P2p spectra in Figure 4.6 iii) shows no apparent shift as well nor a notable difference in the full width at half maximum value. There is no presence of P2p in Graphene as expected that exists in the Gly-Gr interaction. Whereas the nitrogen N1s show a similar interaction where there is no shift in the binding energy as shown in Figure 4.6 iv). Here, the presence of N1s in the Gly-Gr compound can be due to the interaction between the amine, and methylamine functional groups which are present in the glyphosate after the adsorption.⁸⁶

4.3.2 Interaction Glyphosate-Chitosan (Gly-Cs)

An XPS measurement was performed as well to analyze the interaction between glyphosate (Gly) and chitosan (Cs) before and after the absorption of glyphosate in an aqueous medium. Figure 4.7 displays the XPS survey spectra for chitosan, glyphosate, and the interaction of glyphosate-chitosan respectively. In the figure is observable the presence of oxygen, nitrogen, carbon, and phosphorus. Hence, these are the zones that are going to be studied in more detail through a high-resolution measurement.

When observing Figure 4.8 i), it is likely to observe that the carbon C1s region spectra show a greater

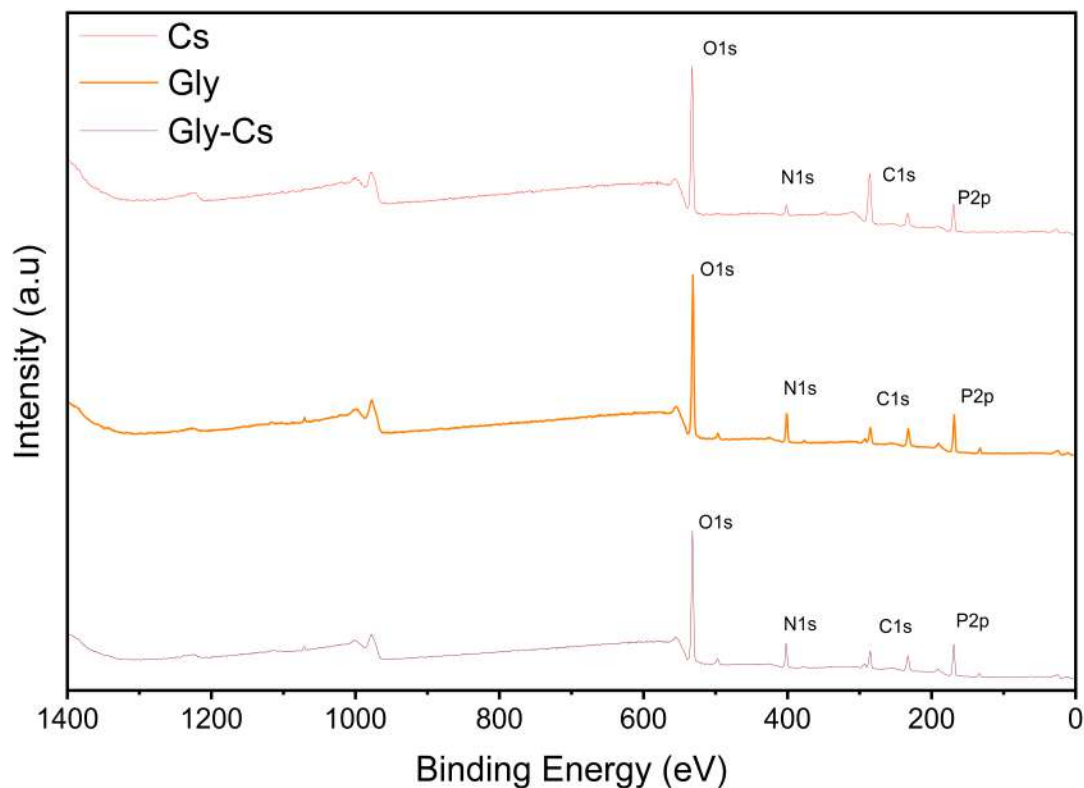


Figure 4.7: X-ray photoelectron survey spectrum of chitosan (Cs), Glyphosate (Gly), and Glyphosate-Chitosan (Gly-Cs).

interaction through functional groups since there is a considerable change in the shape of the spectra comparing chitosan (Cs) with the glyphosate-chitosan interaction (Gly-Cs). This is due to the strong relationship between some functional groups in the adsorption process. There is no evident shift between the binding energies comparing Gly and Gly-Cs, while there is a change in the atomic concentration represented by the area of each component of the C1s spectra. Similarly, Table 4.3 displays the atomic concentration of each assignment for the C1s spectra and their difference from each other. We have, the C-C/C-H main bonding located at 284.6 eV. At this point is observed an increment comparing Gly

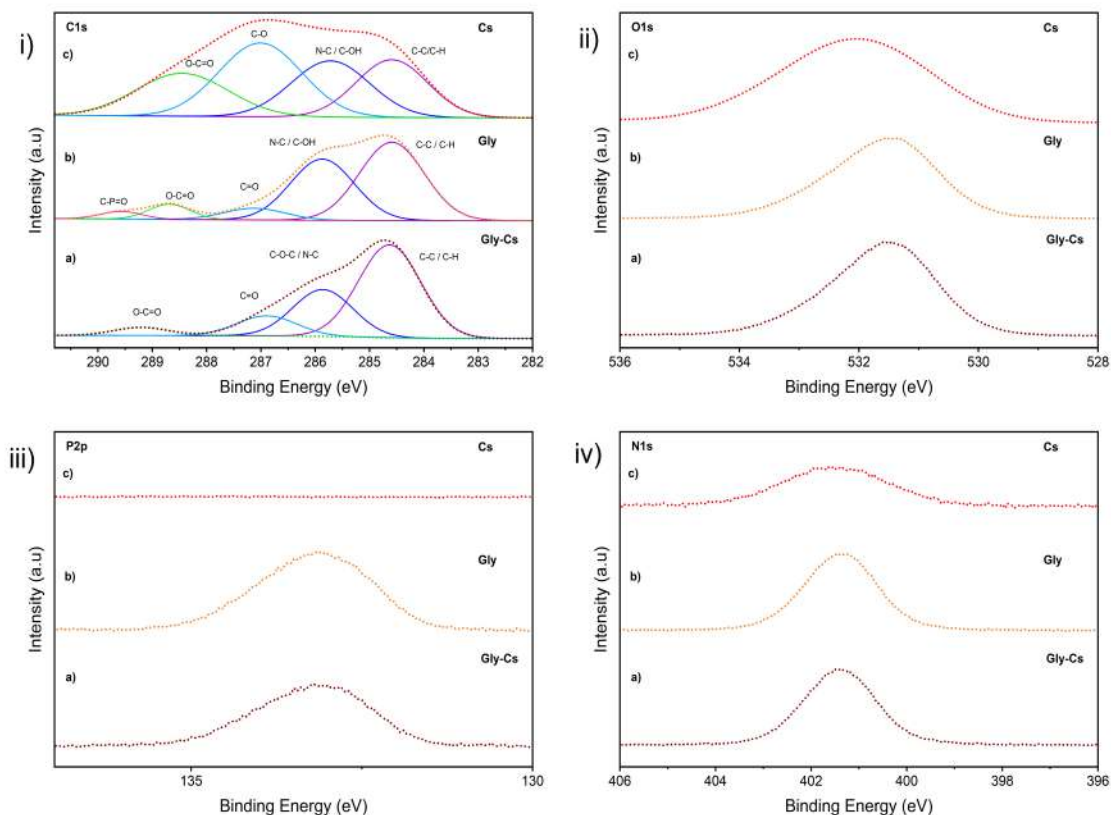


Figure 4.8: X-ray photoelectron high-resolution spectrum of glyphosate (Gly) a), glyphosate-graphene (Gly-Gr) b), and graphene (Gr) c) in the areas of carbon C1s i), oxygen O1s ii), phosphorus P2p iii), and nitrogen N1s iv).

with Gly-Cs shows that there is a strong interaction in this area. Another interesting point occurs around 285.9 eV assigned to the C=O group. Here, the atomic concentration increases in Gly-Cs compared to sole Gly as well. This shows as well an effective interaction of the carboxyl, amine, and phosphate groups in the C1s zone.^{73,86,98}

Table 4.3: C1s Atomic concentrations of chitosan (Gr), glyphosate (Gly), and glyphosate-chitosan (Gly-Gr)

C1s Binding Energies-Atomic Concentration(%)			
Chitosan(Cs)	Glyphosate (Gly)	Glyphosate-Chitosan (Gly-Cs)	Assignment
22.15	47,67	56.56	C=C / C-C / C-H
23.70	36,75	27.45	C-O / N-C / C-OH / C-O-C
32.88	6,70	11.65	C=O
21.25	5,90	4.32	O-C=O
	2,95		C-P=O

The interaction in the O1s, P2p, and N1s zones can be observed in Figure 4.8 ii), iii), and iv) respectively where there is a similar behavior between each of them. Something interesting happens in the O1s area 4.8 ii), where we can observe that the Cs spectra have an ample full width at half maximum value that can be attributed to the bigger presence of oxygen-related groups. Something that can be confirmed in the C1s spectra for chitosan, which also has a bigger area. The Gly and Gly-Cs peaks remain almost unchanged with no difference in the FWHM value. This indicates the interaction of the functional groups present in the adsorption process of glyphosate.

Then, in the P2p spectra 4.8 iii), the contribution can be attributed to glyphosate since no phosphorus is present in the chitosan. Finally, in the N1s area 4.8 iv), the contribution from the chitosan is minimal, and again, the presence of N1s in Gly-Cs can be attributed to the amine, and methylamine functional groups present in the glyphosate molecule.^{99 86}

4.3.3 Interaction Glyphosate-Cobalt Ferrite (Gly-Co)

Now, to analyze the interaction between cobalt ferrite Co and glyphosate Gly, first, a survey XPS spectra was obtained for both Co and Gly and the interaction between them (Gly-Co) as shown in Figure 4.9. There are some things to remark on this figure. The first one is that there is the presence of Co2p and Fe2p3 in the Co spectra whereas in the interaction Gly-Co it is not. This may be caused by the superposition of some particles over these regions, as well as the low concentration of cobalt ferrite nanoparticles. Again, the main zones of interest to be analyzed through a high-resolution spectrum are the C1s, O1s, P2p, Co2p, and Fe2p3.

Figure 4.10 i) represents the interaction in the C1s region. Here, is easy to observe some considerable changes in the atomic concentration of some groups as shown in Table 4.4. These changes are mainly

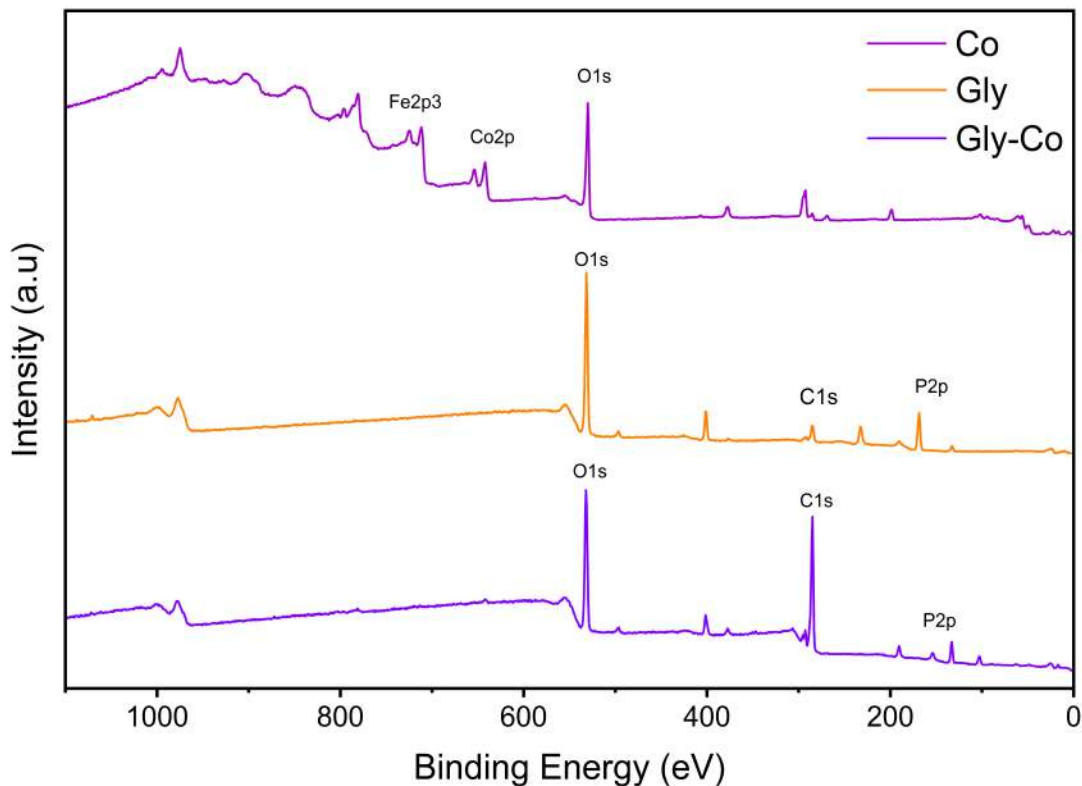


Figure 4.9: X-ray photoelectron survey spectrum of cobalt ferrite (Co), glyphosate (Gly), and glyphosate-cobalt ferrite (Gly-Co).

associated with the presence of oxygen in the cobalt ferrite sample and can be seen in the O1s region displayed in Figure 4.10 ii). Here, for the cobalt ferrite is observed in 4.10 ii)c) the main peak at 529.51 which was attributed to the oxygen lattice. Then, the second peak at 530.96 assigned to a metal-oxygen bonding which corresponds to the bonding between cobalt-oxygen and iron-oxygen observed as well in 4.10 iv) at 795.5 eV for Co-O and 724.04 eV for Fe-O respectively. Finally, the third peak around 532 corresponds to the hydroxyl groups.^{100 101 102}

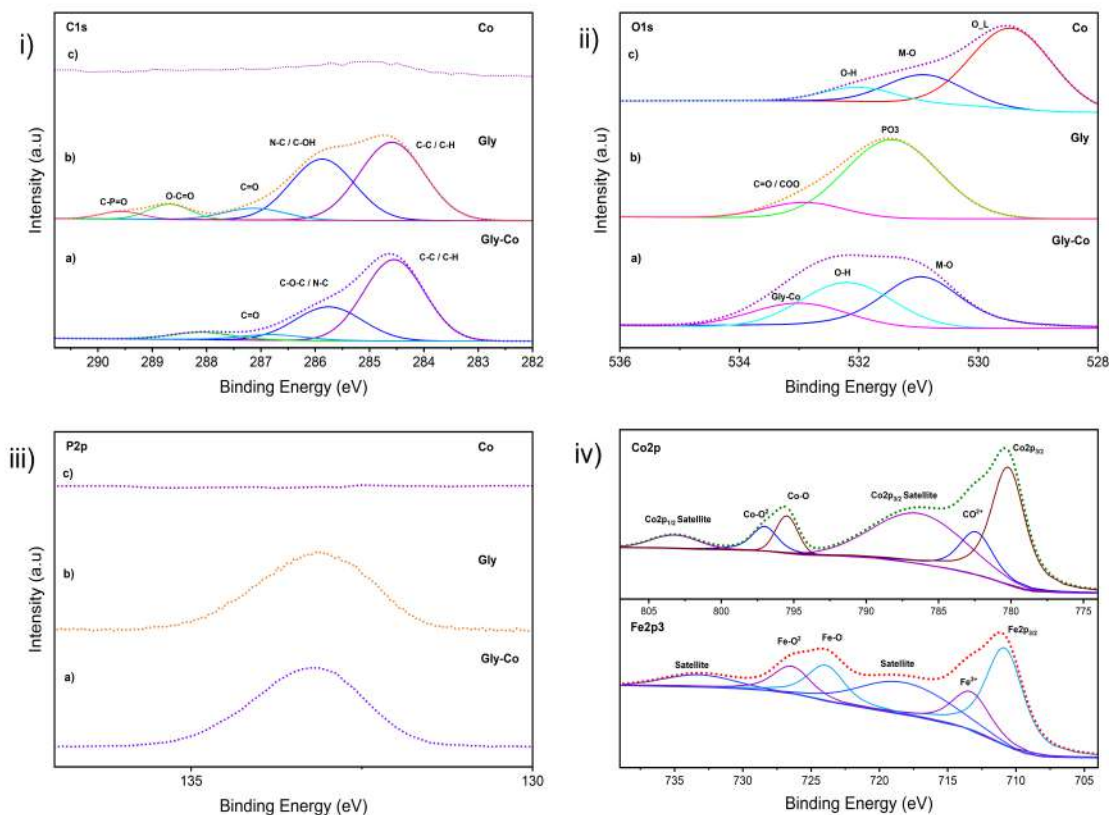


Figure 4.10: X-ray photoelectron high-resolution spectrum of cobalt ferrite (Co) a), glyphosate (Gly) b), and glyphosate-cobalt ferrite (Gly-Co) c) in the regions of carbon C1s i), oxygen O1s ii), phosphorus P2p iii), and the high-resolution spectrum for the cobalt ferrite (Co) in the Co2p and Fe2p3 regions iv).

Table 4.4: C1s Atomic concentrations of cobalt ferrite (Co), glyphosate (Gly), and glyphosate-cobalt ferrite (Gly-Co)

C1s Binding Energies-Atomic Concentration(%)		
Gyphosate (Gly)	Glyphosate-Cobalt Ferrite (Gly-Co)	Assignment
47.67	61.14	C-C / C-H
36.75	28.32	N-C / C-OH/ C-O-C
6.70	5.71	C=O

Even though in the XPS spectra obtained for the interaction, Gly-Co in Figure 4.10ii) a) there is no apparent presence of Co2p and Fe2p3, is shown that the peak for the metal-oxygen bonding is still present. Also, the peak at 532 remains and has an increased atomic concentration as shown in Table 4.5, while there is another peak around 533 assigned to the chemical bonding between glyphosate and the cobalt ferrite surface that matches the peak in Figure 4.10 ii)b) corresponding to the carboxyl groups of glyphosate showing a probable interaction in these regions. Additionally, there is no noticeable change in the FWHM value when comparing the P2p region for Gly, and Gly-Co observed in Figure 4.10 iii)

Table 4.5: O1s Atomic concentrations of cobalt ferrite (Co), glyphosate (Gly), and glyphosate-cobalt ferrite (Gly-Co)

O1s Binding Energies-Atomic Concentration(%)			
Cobalt Ferrite(Co)	Gyphosate (Gly)	Glyphosate-Cobalt Ferrite (Gly-Co)	Assignment
22.42		43.39	M-O
10.30		36.15	O-H
	14.47	20.44	Gly-Co / C-O / COO

4.3.4 Interaction Glyphosate-Nanocomposite (Gly-Nc)

Finally, an analysis was carried out over the interaction between the whole nanocomposite containing graphene, chitosan, and cobalt ferrite CoFe_2O_4 with glyphosate. In order to do so, an XPS survey was performed as well deployed in Figure 4.11. Something interesting found in this plot is the absence of cobalt and iron in the nanocomposite that is supposed to have cobalt ferrite. This can be due to the superposition of other compounds over the surface of the nanocomposite. Again, the regions of interest will be the C1s, O1s, P2p, and N1s regions.

Beginning with the C1s region observed in Figure 4.12i) is likely observed that similar to the graphene case, there are peaks that increase their atomic concentration, showing a potential chemical relation in this area. By referring to Table 4.6 the variation in the concentration for each peak is observed. The first peak around 284.69 eV which corresponds to carbon atoms C-C / C=C increases its concentration in Gly-Nc when compared to Gly, and can be due to the contribution from the nanocomposite. The second peak which is located around 285.9 eV is assigned to the N-C/C-OH / C-O-C groups and is remarkable to notice that the concentration increases in Gly-Nc, potentially due to the bonding with glyphosate in this region. Finally, the atomic concentration in the peaks around 287 eV, and 287.9 eV attributed to C=O, and O-C=O respectively, increases as well in Gly-Nc compared to the sole nanocomposite. These interactions show a

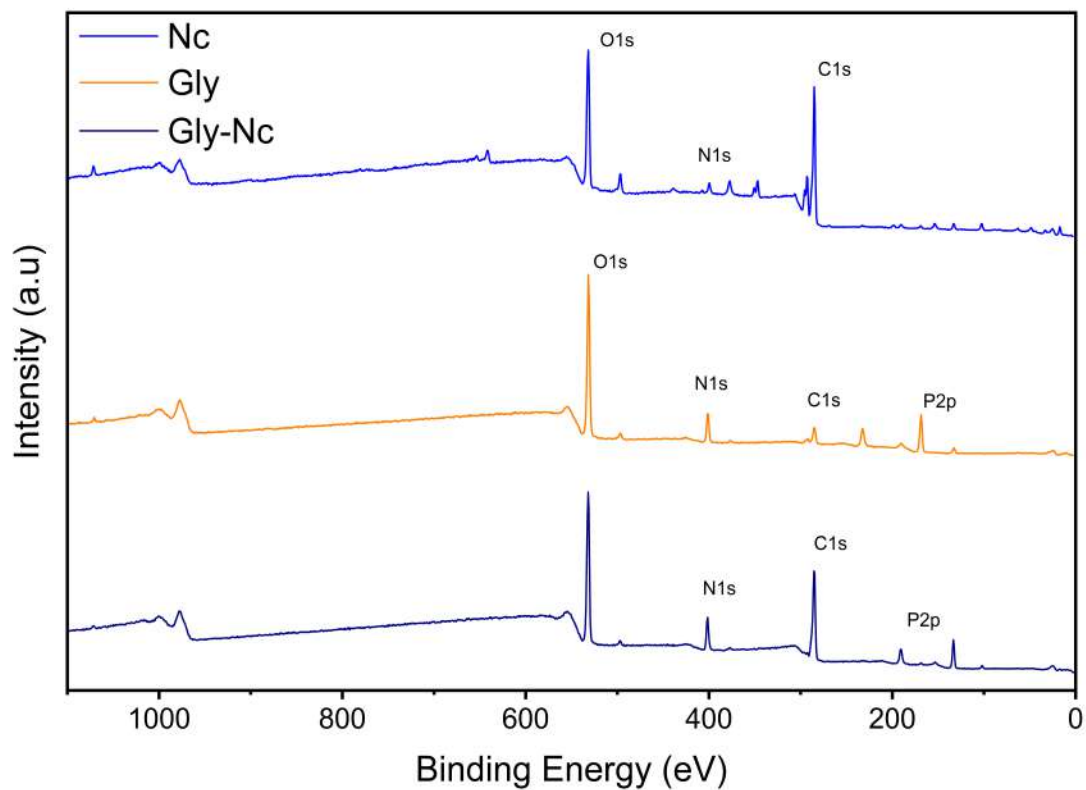


Figure 4.11: X-ray photoelectron survey spectrum of the nanocomposite (Nc), glyphosate (Gly), and glyphosate-nanocomposite (Gly-Nc).

chemical interaction between the carboxyl, and amine groups present in the glyphosate.

Table 4.7: O1s Atomic concentrations of the nanocomposite (Nc), glyphosate (Gly), and glyphosate-nanocomposite (Gly-Nc)

O1s Binding Energies-Atomic Concentration(%)			
Nanocomposite (Nc)	Gyphosate (Gly)	Glyphosate-Nanocomposite (Gly-Nc)	Assignment
69.44	85.52	60.94	O-H / C-O / PO3
24.56	14.47	35.28	N-C / C-OH/ C-O-C
5.99		3.76	O-C=O

Table 4.6: C1s Atomic concentrations of the nanocomposite (Nc), glyphosate (Gly), and glyphosate-nanocomposite (Gly-Nc)

C1s Binding Energies-Atomic Concentration(%)			
Nanocomposite (Nc)	Gyphosate (Gly)	Glyphosate-Nanocomposite (Gly-Nc)	Assignment
64.58	47.67	55.99	C-C / C-H
14.60	36.75	20.26	N-C / C-OH/ C-O-C
9.42	6.70	11.25	C=O
3.54	5.9	5.24	O-C=O

Similarly, The interaction can be observed as well in the O1s region displayed in Figure 4.12ii). Then, as displayed in Table 4.7, in this region is observed an increase in the atomic concentration for each assignment. The second peak located around 532.9 assigned to the carboxyl group shows an increase in Gly-Nc compared to the sole Gly and Nc showing a chemical interaction in this area. Something additional to notice is that, even though there is no presence of cobalt and iron in the Nc sample, it is observable a peak around 534.22 which corresponds to oxygen atoms associated with metal-oxygen bonds. This confirms the presence of cobalt ferrite in the nanocomposite and in the Gly-Nc sample.

Referring to Figure 4.12 iii) and iv) there is no apparent change observed in the FWHM value for P2p and N1s, here the contribution of N1s from the nanocomposite is low and can be attributed to the chitosan. Hence, it is not viable to affirm that there is a direct interaction in these regions but the presence of the PO3 in the O1s region confirms that there is an interaction attributed to the phosphate group present in the glyphosate.⁸⁶

Furthermore, the chemical adsorption of the glyphosate can also be caused by the interaction of the phosphate group which can be with the iron and cobalt nanoparticles present in the cobalt ferrite. This may be observed in the O1s region of the Gly-Co relation in Figure 4.10ii)a) where the M-O bonding is

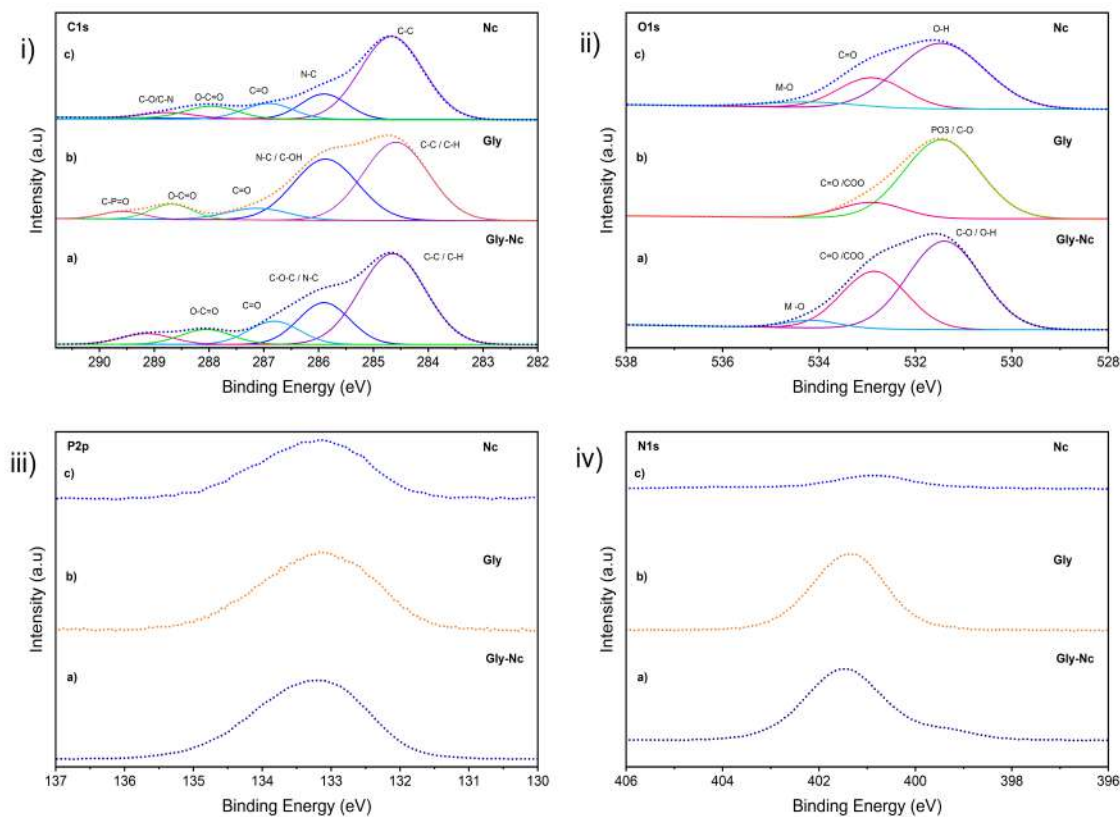


Figure 4.12: X-ray photoelectron high-resolution spectrum of the nanocomposite (Nc) a), glyphosate (Gly) b), and glyphosate-nanocomposite (Gly-Nc) c) in the regions of carbon C1s i), oxygen O1s ii), phosphorus P2p iii), and nitrogen N1s iv).

present as well. This is in accordance with Briceño, S Reinoso. C., 2022 where it is reported that the removal efficacy increases from 48% to 99% after using the cobalt ferrite CoFe_2O_4 nanoparticles.⁸

Chapter 5

Conclusions & Outlook

In this work, the analysis using the spectroscopy techniques RAMAN, FTIR, and X-ray photoelectron spectroscopy is employed to study the possible chemical interaction between glyphosate, a nanocomposite, and each one of its components (graphene, chitosan, and cobalt ferrite).

In the RAMAN spectroscopy, it was possible to observe the peaks associated with the structure of graphene in the nanocomposite, as well as in the Gly-Nc sample. This is attributed to the graphene being the core structure of the nanocomposite. As well, some peaks are identified as the functional groups C-H, COO, C-C, C-O-C, and P-O present in the chitosan and glyphosate. These peaks are observed as well later in the XPS high-resolution spectra for C1s, and O1s regions. In the FTIR analysis, the analysis of the interaction between the nanoparticles forming the nanocomposite and the exchange of functional groups between these components is shown in Figure 4.3, and in Figure 4.4 where it is observed an interaction between each component of the nanocomposite with the glyphosate thanks to the presence of the peaks related to the glyphosate in the interaction Gly-Nc where they appear with a sharpened peak showing a change in its chemical composition. In this plot is necessary to notice that there is a bigger interaction associated with the phosphate group, present in the glyphosate. This relation is possibly caused by the interaction of the phosphate group with the metal ions present in the cobalt ferrite which is part of the nanocomposite. This can be observed as well in the XPS high resolution for O1s in Figure 4.12 ii). Finally, the XPS analysis is the most extensive of the three. Here, it is possible to study in a high-resolution spectrum the binding energies associated with each one of the components of the nanocomposite and their interaction with glyphosate. Is possible to observe that the associated peaks found after the fitting in the C1s, and O1s regions are in accordance with the peaks found in the RAMAN, and FTIR analysis. Also, there are changes observed in the atomic concentration of some of these peaks which indicates an effective

chemical interaction in these regions.

Thanks to the effective usage of RAMAN, FTIR, and X-ray photoelectron spectroscopy, it was successfully performed a step-by-step analysis to show a chemical and molecular interaction between each one of the components of the nanocomposite. The results show that there is indeed an interaction between the glyphosate molecule, the nanocomposite, and each one of its components. This can be mainly observed through the XPS analysis which shows the different binding interactions corresponding to the composition of each molecule. This allows a better understanding of the mechanism behind the interactions present in the removal process of glyphosate using the nanocomposite made of graphene, chitosan, and cobalt ferrite nanoparticles.

Bibliography

- [1] Cao, L.; Ma, D.; Zhou, Z.; Xu, C.; Cao, C.; Zhao, P.; Huang, Q. Efficient photocatalytic degradation of herbicide glyphosate in water by magnetically separable and recyclable BiOBr/Fe₃O₄ nanocomposites under visible light irradiation. *Chemical Engineering Journal* **2019**, *368*, 212–222.
- [2] Casabé, N.; Piola, L.; Fuchs, J.; Oneto, M. L.; Pamparato, L.; Basack, S.; Giménez, R.; Massaro, R.; Papa, J. C.; Kesten, E. Ecotoxicological assessment of the effects of glyphosate and chlorpyrifos in an Argentine soya field. *Journal of Soils and Sediments* **2007**, *7*, 232–239.
- [3] Bradberry, S. M.; Proudfoot, A. T.; Vale, J. A. Glyphosate poisoning. *Toxicological Reviews* **2004**, *23*, 159–167.
- [4] Bermeo, J. “ Repercusiones jurídicas de las fumigaciones con glifosato a los cultivos ilícitos en Colombia y el impacto ambiental en la frontera colombo ecuatoriana ” Quito. *Uce* **2014**,
- [5] Carlisle, S.; Trevors, J. Glyphosate in the environment. *Water, Air, and Soil Pollution* **1988**, *39*, 409–420.
- [6] Xue, L.; Hao, L.; Ding, H.; Liu, R.; Zhao, D.; Fu, J.; Zhang, M. Complete and rapid degradation of glyphosate with Fe₃Ce₁O_x catalyst for peroxymonosulfate activation at room temperature. *Environmental Research* **2021**, *201*, 111618.
- [7] Páez, M. R.; Ochoa-Muñoz, Y.; Rodríguez-Páez, J. E. Efficient removal of a glyphosate-based herbicide from water using ZnO nanoparticles (ZnO-NPs). *Biocatalysis and Agricultural Biotechnology* **2019**, *22*, 101434.
- [8] Briceño, S.; Reinoso, C. CoFe₂O₄-chitosan-graphene nanocomposite for glyphosate removal. *Environmental Research* **2022**, *212*.

- [9] Arias, F. A.; Guevara, M.; Tene, T.; Angamarca, P.; Molina, R.; Valarezo, A.; Salguero, O.; Gomez, C. V.; Arias, M.; Caputi, L. S. The adsorption of methylene blue on eco-friendly reduced graphene oxide. *Nanomaterials* **2020**, *10*.
- [10] Hakeem, K. R.; Akhtar, M. S.; Abdullah, S. N. A. Plant, soil and microbes: Volume 1: Implications in crop science. *Plant, Soil and Microbes: Volume 1: Implications in Crop Science* **2016**, 1–366.
- [11] Pell, M.; Stenberg, B.; Torstensson, L. Potential denitrification and nitrification tests for evaluation of pesticide effects in soil. *Ambio* **1998**, 24–28.
- [12] Dich, J.; Zahm, S. H.; Hanberg, A.; Adami, H. O. Pesticides and cancer. *Cancer Causes and Control* **1997**, *8*, 420–443.
- [13] Duke, S. O. The history and current status of glyphosate. *Pest Management Science* **2018**, *74*, 1027–1034.
- [14] Prasad, S.; Srivastava, S.; Singh, M.; Shukla, Y. Clastogenic Effects of Glyphosate in Bone Marrow Cells of Swiss Albino Mice. *Journal of Toxicology* **2009**, *2009*, 1–6.
- [15] Maggi, F.; la Cecilia, D.; Tang, F. H.; McBratney, A. The global environmental hazard of glyphosate use. *Science of the Total Environment* **2020**, *717*, 137167.
- [16] Thakur, D. S.; Khot, R.; Joshi, P.; Pandharipande, M.; Nagpure, K. Glyphosate poisoning with acute pulmonary edema. *Toxicology international* **2014**, *21*, 328.
- [17] Annett, R.; Habibi, H. R.; Hontela, A. Impact of glyphosate and glyphosate-based herbicides on the freshwater environment. *Journal of Applied Toxicology* **2014**, *34*, 458–479.
- [18] Richmond, M. E. Glyphosate: A review of its global use, environmental impact, and potential health effects on humans and other species. *Journal of Environmental Studies and Sciences* **2018**, *8*, 416–434.
- [19] Maldonado, A. Los impactos de las fumigaciones en la frontera ecuatoriana. *Ecología política* **2001**, 61–72.
- [20] Talbot, A. R.; Shiaw, M. H.; Huang, J. S.; Yang, S. F.; Goo, T. S.; Wang, S. H.; Chen, C. L.; Sanford, T. R. Acute Poisoning with a Glyphosate-Surfactant Herbicide ('Roundup'): A Review of 93 Cases. *Human Experimental Toxicology* **1991**, *10*, 1–8.

- [21] Paz-y Miño, C.; Sánchez, M. E.; Arévalo, M.; Muñoz, M. J.; Witte, T.; De-la Carrera, G. O.; Leone, P. E. Evaluation of DNA damage in an Ecuadorian population exposed to glyphosate. *Genetics and Molecular Biology* **2007**, *30*, 456–460.
- [22] Titirici, M.-M.; White, R. J.; Brun, N.; Budarin, V. L.; Su, D.-S.; Del Monte, F.; Clark, J. H.; MacLachlan, M. J. Sustainable Carbon Materials Chemical Society Reviews Sustainable Carbon Materials. *Chemical Society Reviews* **2014**,
- [23] Zhang, L.; Zhao, X. S. Carbon-based materials as supercapacitor electrodes. *Chemical Society Reviews* **2009**, *38*, 2520–2531.
- [24] Visakh, P. Introduction for nanomaterials and nanocomposites: state of art, new challenges, and opportunities. *Nanomaterials and Nanocomposites: Zero-to Three-Dimensional Materials and Their Composites* **2016**, 1–20.
- [25] Toto, E.; Laurenzi, S.; Santonicola, M. G. Recent Trends in Graphene/Polymer Nanocomposites for Sensing Devices: Synthesis and Applications in Environmental and Human Health Monitoring. *Polymers* **2022**, *14*.
- [26] Geim, A. K.; Novoselov, K. S. The rise of graphene. *Nature materials* **2007**, *6*, 183–191.
- [27] Huang, Y.; Liang, J.; Chen, Y. An overview of the applications of graphene-based materials in supercapacitors. *small* **2012**, *8*, 1805–1834.
- [28] Gopinath, K. P.; Vo, D. V. N.; Gnana Prakash, D.; Adithya Joseph, A.; Viswanathan, S.; Arun, J. Environmental applications of carbon-based materials: a review. *Environmental Chemistry Letters* **2021**, *19*, 557–582.
- [29] Tene, T.; Guevara, M.; Valarezo, A.; Salguero, O.; Arias Arias, F.; Arias, M.; Scarcello, A.; Caputi, L. S.; Vacacela Gomez, C. Drying-time study in graphene oxide. *Nanomaterials* **2021**, *11*, 1–14.
- [30] Dasari, B. L.; Nouri, J. M.; Brabazon, D.; Naher, S. Graphene and derivatives – Synthesis techniques, properties and their energy applications. *Energy* **2017**, *140*, 766–778.
- [31] Seekaew, Y.; Phokharatkul, D.; Wisitsoraat, A.; Wongchoosuk, C. Highly sensitive and selective room-temperature NO₂ gas sensor based on bilayer transferred chemical vapor deposited graphene. *Applied Surface Science* **2017**, *404*, 357–363.

- [32] Seekaew, Y.; Arayawut, O.; Timsorn, K.; Wongchoosuk, C. *Carbon-Based Nanofillers and Their Rubber Nanocomposites: Carbon Nano-Objects*; Elsevier Inc., 2018; pp 259–283.
- [33] Paul, S.; Jayan, A.; Sasikumar, C. S.; Cherian, S. M. Extraction and purification of chitosan from chitin isolated from sea prawn *Fenneropenaeus indicus*. *Extraction* **2014**, *7*, 201–204.
- [34] Kumar, M. N. R. A review of chitin and chitosan applications. *Reactive and functional polymers* **2000**, *46*, 1–27.
- [35] Nilsen-Nygaard, J.; Strand, S. P.; Vårum, K. M.; Draget, K. I.; Nordgård, C. T. Chitosan: Gels and interfacial properties. *Polymers* **2015**, *7*, 552–579.
- [36] Cheba, B. A. Chitin and chitosan: marine biopolymers with unique properties and versatile applications. *Global Journal of Biotechnology & Biochemistry* **2011**, *6*, 149–153.
- [37] Divya, K.; Jisha, M. S. Chitosan nanoparticles preparation and applications. *Environmental Chemistry Letters* **2018**, *16*, 101–112.
- [38] Bárcena, C.; Sra, A. K.; Gao, J. Applications of magnetic nanoparticles in biomedicine. *Nanoscale Magnetic Materials and Applications* **2009**, *167*, 591–626.
- [39] Nalwa, H. S. *Encyclopedia of nanoscience and nanotechnology* (v. 8. *Ne-P*); American scientific publishers, 2004; p 815.
- [40] Leslie-Pelecky, D. L.; Rieke, R. D. Magnetic properties of nanostructured materials. *Chemistry of materials* **1996**, *8*, 1770–1783.
- [41] Soler, M. A.; Paterno, L. G. Magnetic nanomaterials. *Nanostructures* **2017**, *200*, 147–186.
- [42] Vatta, L. L.; Sanderson, R. D.; Koch, K. R. Magnetic nanoparticles: Properties and potential applications. *Pure and Applied Chemistry* **2006**, *78*, 1793–1801.
- [43] Seesod, N.; Nopparat, P.; Hedrum, A.; Holder, A.; Thaithong, S.; Uhlen, M.; Lundeberg, J. An integrated system using immunomagnetic separation, polymerase chain reaction, and colorimetric detection for diagnosis of *Plasmodium falciparum*. *The American journal of tropical medicine and hygiene* **1997**, *56*, 322–328.
- [44] Maaz, K.; Mumtaz, A.; Hasanain, S. K.; Ceylan, A. Synthesis and magnetic properties of cobalt ferrite (CoFe₂O₄) nanoparticles prepared by wet chemical route. *Journal of Magnetism and Magnetic Materials* **2007**, *308*, 289–295.

- [45] Aslibeiki, B.; Kameli, P.; Salamati, H.; Eshraghi, M.; Tahmasebi, T. Superspin glass state in MnFe₂O₄ nanoparticles. *Journal of Magnetism and Magnetic Materials* **2010**, *322*, 2929–2934.
- [46] Pan, X.; Sun, A.; Han, Y.; Zhang, W.; Zhao, X. Structural and magnetic properties of Bi³⁺ ion doped Ni–Cu–Co nano ferrites prepared by sol–gel auto combustion method. *Journal of Materials Science: Materials in Electronics* **2019**, *30*, 4644–4657.
- [47] Safdari, M.; Al-Haik, M. S. *Carbon-Based Polymer Nanocomposites for Environmental and Energy Applications*; Elsevier Inc., 2018; pp 113–146.
- [48] Mohanty, S.; Chakraborty, S.; Das, M.; Paul, S. Role of nanomaterials in phytoremediation of tainted soil. *Phytoremediation Technology for the Removal of Heavy Metals and Other Contaminants from Soil and Water* **2022**, 329–353.
- [49] Saikia, P. Clay nanostructures for biomedical applications. *Two-Dimensional Nanostructures for Biomedical Technology: A Bridge between Material Science and Bioengineering* **2020**, 137–172.
- [50] Potts, J. R.; Dreyer, D. R.; Bielawski, C. W.; Ruoff, R. S. Graphene-based polymer nanocomposites. *Polymer* **2011**, *52*, 5–25.
- [51] Chen, D.; Feng, H.; Li, J. Graphene oxide: Preparation, functionalization, and electrochemical applications. *Chemical Reviews* **2012**, *112*, 6027–6053.
- [52] hai Yang, G.; dan Bao, D.; Liu, H.; qing Zhang, D.; Wang, N.; tao Li, H. Functionalization of Graphene and Applications of the Derivatives. *Journal of Inorganic and Organometallic Polymers and Materials* **2017**, *27*, 1129–1141.
- [53] Masoumparast, M.; Mokhtary, M.; Kefayati, H. Preparation and characterization of polyvinylpyrrolidone/cobalt ferrite functionalized chitosan graphene oxide (CoFe₂O₄@CS@GO-PVP) nanocomposite. *Journal of Polymer Engineering* **2020**, *40*, 342–349.
- [54] Debnath, S.; Maity, A.; Pillay, K. Magnetic chitosan–GO nanocomposite: Synthesis, characterization and batch adsorber design for Cr(VI) removal. *Journal of Environmental Chemical Engineering* **2014**, *2*, 963–973.
- [55] Raman, C. V.; Krishnan, K. S. A new type of secondary radiation. *Nature* **1928**, *121*, 501–502.
- [56] Long, D. A. Raman spectroscopy. *New York* **1977**, *1*.

- [57] Smith, E.; Dent, G. Wiley Ed. *Modern Raman Spectroscopy: A Practical Approach* **2005**, *1*, 224.
- [58] Graves, P.; Gardiner, D. *Practical raman spectroscopy*. Springer **1989**, *10*, 978–3.
- [59] Luisetto, M. Raman (Rs) Spectroscopy for Biopharmaceutical Quality Control and PAT. Raw Material - Final Products: the Nanolipids Effect on Signal Intensity. Regulatory and Toxicological Aspects. *Medicinal Analytical Chemistry International Journal* **2022**, *6*.
- [60] Edwards, H. G. M. *Journal of Raman Spectroscopy*; 2005; Vol. 36; pp 835–835.
- [61] Jorio, A. Raman Spectroscopy in Graphene-Based Systems: Prototypes for Nanoscience and Nanometrology. *ISRN Nanotechnology* **2012**, *2012*, 1–16.
- [62] Qu, S.; Wu, G.; Fang, J.; Zang, D.; Xing, H.; Wang, L.; Wu, H. *Spectroscopic Methods for Nanomaterials Characterization*; 2017; Vol. 2; pp 301–319.
- [63] Ganzoury, M. A.; Allam, N. K.; Nicolet, T.; All, C. Introduction to Fourier Transform Infrared Spectrometry. *Renewable and Sustainable Energy Reviews* **2015**, *50*, 1–8.
- [64] Smith, B. C. *Fundamentals of Fourier Transform Infrared Spectroscopy, Second Edition*; 2011; pp 1–183.
- [65] Low, W.; M.Schieber, *Applied Solid State*; 1970.
- [66] Griffiths, P. R. The origin of Fourier transform techniques for the measurement of high-quality infrared spectra can be traced back to. **1983**, 297–302.
- [67] Kuptsov, A. H.; Zhizhin, G. N. G. N. Handbook of fourier transform Raman and infrared spectra of polymers. **1998**, 536.
- [68] Ferraro, J. R. History of Fourier transform-infrared spectroscopy. *Spectroscopy (Santa Monica)* **1999**, *14*, 28–40.
- [69] Zhang, T. *Synchrotron Radiation Studies of Molecular Building Blocks for Functional Materials*; 2018; p 97.
- [70] Kuzmany, H. *Solid-State Spectroscopy*; 2009.
- [71] Van der Heide, P. *X-ray photoelectron spectroscopy: an introduction to principles and practices*; John Wiley & Sons, 2011.

- [72] Cushman, C. V.; Chatterjee, S.; Major, G. H.; Smith, N. J.; Roberts, A.; Linford, M. R. Trends in Advanced XPS Instrumentation. I. Overview of the Technique, Automation, High Sensitivity, Imaging, Snapshot Spectroscopy, Gas Cluster Ion Beams, and Multiple Analytical Techniques on the Instrument. *Vacuum Technology Coating* **2016**, 2–9.
- [73] Chastain, J.; King Jr, R. C. Handbook of X-ray photoelectron spectroscopy. *Perkin-Elmer Corporation* **1992**, 40, 221.
- [74] Haberer, D. Electronic Properties of Functionalized Graphene Studied With Electronic Properties of Functionalized Graphene Studied With Photoemission Spectroscopy at Mathematik und Naturwissenschaften der Technischen Universität. **2014**,
- [75] Shinotsuka, H.; Yoshikawa, H.; Murakami, R.; Nakamura, K.; Tanaka, H.; Yoshihara, K. Automated information compression of XPS spectrum using information criteria. *Journal of Electron Spectroscopy and Related Phenomena* **2020**, 239, 146903.
- [76] Major, G. H.; Fairley, N.; Sherwood, P. M. A.; Linford, M. R.; Terry, J.; Fernandez, V.; Artyushkova, K. Practical guide for curve fitting in x-ray photoelectron spectroscopy. *Journal of Vacuum Science Technology A* **2020**, 38, 061203.
- [77] others., *et al.* Practical guides for x-ray photoelectron spectroscopy: First steps in planning, conducting, and reporting XPS measurements. *Journal of Vacuum Science & Technology A: Vacuum, Surfaces, and Films* **2019**, 37, 031401.
- [78] Gupta, V.; Ganegoda, H.; Engelhard, M. H.; Terry, J.; Linford, M. R. Assigning oxidation states to organic compounds via predictions from X-ray photoelectron spectroscopy: a discussion of approaches and recommended improvements. *Journal of Chemical Education* **2014**, 91, 232–238.
- [79] Watts, J. F.; Wolstenholme, J. *An introduction to surface analysis by XPS and AES*; John Wiley & Sons, 2019.
- [80] Jain, V.; Biesinger, M. C.; Linford, M. R. The Gaussian-Lorentzian Sum, Product, and Convolution (Voigt) functions in the context of peak fitting X-ray photoelectron spectroscopy (XPS) narrow scans. *Applied Surface Science* **2018**, 447, 548–553.
- [81] Fairley, N.; Carrick, A.; Fairly, N. *The casa cookbook*; Acolyte science Cheshire, 2005; Vol. 1.

- [82] Wang, K.; Ma, Q.; Pang, K.; Ding, B.; Zhang, J.; Duan, Y. One-pot synthesis of graphene/chitin nanofibers hybrids and their remarkable reinforcement on Poly(vinyl alcohol). *Carbohydrate Polymers* **2018**, *194*, 146–153.
- [83] Ferrari, A. C.; Meyer, J. C.; Scardaci, V.; Casiraghi, C.; Lazzeri, M.; Mauri, F.; Piscanec, S.; Jiang, D.; Novoselov, K. S.; Roth, S.; Geim, A. K. Raman spectrum of graphene and graphene layers. *Physical Review Letters* **2006**, *97*, 1–4.
- [84] Mishra, A.; Singh, V. K.; Mohanty, T. Coexistence of interfacial stress and charge transfer in graphene oxide-based magnetic nanocomposites. *Journal of Materials Science* **2017**, *52*, 7677–7687.
- [85] Xu, M. L.; Gao, Y.; Jin, J.; Xiong, J. F.; Han, X. X.; Zhao, B. Role of 2-13 c isotopic glyphosate adsorption on silver nanoparticles based on ninhydrin reaction: A study based on surface—enhanced raman spectroscopy. *Nanomaterials* **2020**, *10*, 1–11.
- [86] Ramrakhiani, L.; Ghosh, S.; Mandal, A. K.; Majumdar, S. Utilization of multi-metal laden spent biosorbent for removal of glyphosate herbicide from aqueous solution and its mechanism elucidation. *Chemical Engineering Journal* **2019**, *361*, 1063–1077.
- [87] Kumar, Y.; Shirage, P. M. Highest coercivity and considerable saturation magnetization of CoFe₂O₄ nanoparticles with tunable band gap prepared by thermal decomposition approach. *Journal of Materials Science* **2017**, *52*, 4840–4851.
- [88] Zajac, A.; Hanuza, J.; Wandas, M.; Dymińska, L. Determination of N-acetylation degree in chitosan using Raman spectroscopy. *Spectrochimica Acta - Part A: Molecular and Biomolecular Spectroscopy* **2015**, *134*, 114–120.
- [89] Do, M. H.; Dubreuil, B.; Peydecastaing, J.; Vaca-Medina, G.; Nhu-Trang, T.-T.; Jaffrezic-Renault, N.; Behra, P. Chitosan-based nanocomposites for glyphosate detection using surface plasmon resonance sensor. *Sensors* **2020**, *20*, 5942.
- [90] Gaffney, J. S.; Marley, N. A.; Jones, D. E. Fourier transform infrared (FTIR) spectroscopy. *Characterization of materials* **2002**, 1–33.
- [91] S. Dassanayake, R.; Acharya, S.; Abidi, N. Biopolymer-Based Materials from Polysaccharides: Properties, Processing, Characterization and Sorption Applications. *Advanced Sorption Process Applications* **2019**, 1–24.

- [92] Shariatinia, Z.; Mazloom-Jalali, A. Molecular dynamics simulations on chitosan/graphene nanocomposites as anticancer drug delivery using systems. *Chinese Journal of Physics* **2020**, *66*, 362–382.
- [93] Park, H.; May, A.; Portilla, L.; Dietrich, H.; Münch, F.; Rejek, T.; Sarcletti, M.; Banspach, L.; Zahn, D.; Halik, M. Magnetite nanoparticles as efficient materials for removal of glyphosate from water. *Nature Sustainability* **2020**, *3*, 129–135.
- [94] Ueda Yamaguchi, N.; Bergamasco, R.; Hamoudi, S. Magnetic MnFe₂O₄-graphene hybrid composite for efficient removal of glyphosate from water. *Chemical Engineering Journal* **2016**, *295*, 391–402.
- [95] Duan, G. W.; Zhang, J.; Li, Y.; Xu, Y. M.; Yin, F.; Fu, Y. Z. The preparation of Fe₃O₄/molecular-imprinted nanocomposite and the application on the recognition and separation of glyphosate. *Inorganic and Nano-Metal Chemistry* **2017**, *47*, 481–487.
- [96] Li, X. H.; Xu, C. L.; Han, X. H.; Qiao, L.; Wang, T.; Li, F. S. Synthesis and magnetic properties of nearly monodisperse CoFe₂O₄ nanoparticles through a simple hydrothermal condition. *Nanoscale Research Letters* **2010**, *5*, 1039–1044.
- [97] Stevanović, M.; Djošić, M.; Janković, A.; Kojić, V.; Vukašinović-Sekulić, M.; Stojanović, J.; Odović, J.; Crevar Sakač, M.; Kyong Yop, R.; Mišković-Stanković, V. Antibacterial graphene-based hydroxyapatite/chitosan coating with gentamicin for potential applications in bone tissue engineering. *Journal of Biomedical Materials Research - Part A* **2020**, *108*, 2175–2189.
- [98] Gao, G.; Liu, D.; Tang, S.; Huang, C.; He, M.; Guo, Y.; Sun, X.; Gao, B. Heat-Initiated Chemical Functionalization of Graphene. *Scientific Reports* **2016**, *6*, 1–8.
- [99] Jayasumana, C.; Gunatilake, S.; Senanayake, P. Glyphosate, hard water and nephrotoxic metals: Are they the culprits behind the epidemic of chronic kidney disease of unknown etiology in Sri Lanka. *International Journal of Environmental Research and Public Health* **2014**, *11*, 2125–2147.
- [100] Zhang, Z.; Li, W.; Zou, R.; Kang, W.; San Chui, Y.; Yuen, M. F.; Lee, C. S.; Zhang, W. Layer-stacked cobalt ferrite (CoFe₂O₄) mesoporous platelets for high-performance lithium ion battery anodes. *Journal of Materials Chemistry A* **2015**, *3*, 6990–6997.
- [101] Yadav, R. S.; Kuřitka, I.; Vilcakova, J.; Havlica, J.; Masilko, J.; Kalina, L.; Tkacz, J.; Švec, J.; Enev, V.; Hajdúchová, M. Impact of grain size and structural changes on magnetic, dielectric, electrical, impedance and modulus spectroscopic characteristics of CoFe₂O₄ nanoparticles synthesized

- by honey mediated sol-gel combustion method. *Advances in Natural Sciences: Nanoscience and Nanotechnology* **2017**, 8.
- [102] Lv, H.; Zhao, H.; Cao, T.; Qian, L.; Wang, Y.; Zhao, G. Efficient degradation of high concentration azo-dye wastewater by heterogeneous Fenton process with iron-based metal-organic framework. *Journal of Molecular Catalysis A: Chemical* **2015**, 400, 81–89.